ACR No. L5B01a

NATIONAL ADVISORY COMMITTEE FOR AERONAUTICS

WARTIME REPORT

ORIGINALLY ISSUED
February 1945 as
Advance Confidential Report L5B01a

WIND-TUNNEL INVESTIGATION OF A HIGH-CRITICAL-SPEED FUSELAGE SCOOP INCLUDING THE EFFECTS OF BOUNDARY LAYER

By Norman F. Smith and Donald D. Baals

Langley Memorial Aeronautical Laboratory
Langley Field, Va.

WASHINGTON

NACA ACR No. L5B01a

NATIONAL ADVISORY COMMITTEE FOR AERONAUTICS

ADVANCE CONFIDENTIAL REPORT

WIND-TUNNEL INVESTIGATION OF A HIGH-CRITICAL-SPEED FUSELAGE SCOOP INCLUDING THE EFFECTS OF BOUNDARY LAYER

By Norman F. Smith and Donald D. Baals

SUMMARY

A large air scoop designed for high critical speed has been tested in the Langley 8-foot high-speed tunnel on the fuselage of a $\frac{1}{5}$-scale fighter-type airplane. The scoop inlet area was selected from considerations of the total air requirements for a 2000-horsepower engine. The critical Mach number of the scoop tested (apart from the wing-scoop juncture) was 0.75 at an inlet-velocity ratio of 0.6. This value of critical Mach number decreased to 0.67 at an inlet-velocity ratio of 0.4. A slightly lower critical speed was attained in the wing-scoop juncture. The results of these tests indicated that high-critical-speed scoops can be derived directly from high-critical-speed three-dimensional nose-inlet shapes.

The effects of boundary layer on scoop characteristics were found to be important at all inlet-velocity ratios. At low values of inlet-velocity ratio, the positive pressure gradient ahead of the scoop entrance caused the boundary layer to separate externally; this separation caused significant losses in total pressure in the scoop duct and high external drag. At high inlet-velocity ratios, the boundary-layer air induced separation in the scoop diffuser, which caused appreciable losses in total pressure.

A boundary-layer passage of height twice the normal boundary-layer thickness, when operated at a sufficiently high inlet-velocity ratio, eliminated internal losses due to separation and effected a substantial decrease in drag over that of the original scoop installation.

INTRODUCTION

A research program has been initiated at the Langley 8-foot high-speed tunnel for the development of high-critical-speed, low-drag, fuselage air scoops. Much of the work previously done on air scoops has been confined to the development of specific scoop installations for a given airplane with little consideration for the development of general scoop design criterions. The present investigation was planned to yield results, insofar as possible, that are generally applicable. The tests were made with a generalized fighter-type airplane model constructed to proportions in current use and provided with a means for varying the scoop air-flow quantity through a wide range.

In the first phase of the program, the results of which are reported herein, tests were made of a high-critical-speed air scoop mounted near the midposition on the model fuselage. The purpose of these tests was to determine the effects of fuselage boundary layer on the scoop characteristics, to determine the requirements of passages suitable for removal and disposition of the boundary layer, and to obtain performance data on the first of a series of scoops designed for high critical speed.

SYMBOLS

a_o	speed of sound in free-stream air, feet per second
M_o	free-stream Mach number (V_o/a_o)
M_{cr}	critical Mach number
α	model angle of attack referenced to wing chord line, degrees
ρ_o	free-stream density, slugs per cubic foot
q_o	free-stream dynamic pressure, pounds per square foot $\left(\frac{1}{2}\rho_o V_o^2\right)$

H_o	free-stream total pressure, pounds per square foot
H	local total pressure, pounds per square foot
ΔH	total-pressure loss, pounds per square foot
p_o	free-stream static pressure, pounds per square foot
$\frac{H - p_o}{H_o - p_o}$	total-pressure-recovery ratio
p	local static pressure, pounds per square foot
P	pressure coefficient $\left(\frac{p - p_o}{q_o}\right)$
F_s	scoop maximum frontal area (0.219 sq ft)
S	wing area (13.85 sq ft)
D	drag, pounds
D_{int}	internal drag (to rake station), pounds
C_D	drag coefficient $\left(\frac{D}{q_o S}\right)$
C_{D_F}	scoop external-drag coefficient $\left(\frac{D_s - D_{int}}{q_o F_s}\right)$
R	Reynolds number, based on fuselage length of 6.66 feet
V_o	free-stream velocity, feet per second
V_1	velocity at scoop entrance, feet per second
V_1/V_o	scoop inlet-velocity ratio
$(V_1/V_o)_{BL}$	boundary-layer-passage inlet-velocity ratio
δ	boundary-layer thickness
l	length
δ/l_f	nondimensional boundary-layer thickness
x	horizontal distance along model reference line

in the tunnel test section is shown in figure 2. The fuselage fineness ratios (plan and side views), wing location, chord, and thickness ratio were chosen as representative of values used in current designs. A canopy installation was omitted because its effect on the present scoop installation was not considered significant. The fuselage outlines are symmetrical in side and plan views and were derived from the NACA 111 body ordinates (reference 1). The fuselage cross section at every station was composed of two semicircles of radius w_f, connected by straight lines. (See front view, fig. 1.) The wing section is an NACA 66(215)-114 airfoil section (reference 2) set at an angle of incidence of 1°. Ordinates for the wing and fuselage are given in table I.

A scale drawing showing the arrangement and principal dimensions of the scoop installation is presented in figure 3. The scoop entrance was located at the wing 60-percent-chord station; the maximum section, at the wing trailing edge. The scoop section was semicircular with vertical side walls intersecting the wing and fuselage. The maximum width of the scoop body was equal to the maximum width of the fuselage, and the maximum depth (below the fuselage bottom surface) was equal to one-half the fuselage maximum width. The inlet area was fixed at 0.078 square feet model scale or 1.95 square feet full scale to be in the range required for current installations of 2000 horsepower.

The scoop-forebody ordinates (between the entrance and the maximum scoop section) were derived from nose B of reference 3. The nose B profile of reference 3 was considered to extend back to the maximum section of the original streamline body to which it was attached. The resulting ordinates were modified slightly behind the nose section to improve the fairing and were then applied in a nondimensional form to the scoop profile between the inlet and the maximum-diameter stations. The original nose B installation and final scoop dimensions were as follows:

	Original nose B (reference 3)	Scoop
d/D	0.38	0.625
X/D	1.85	1.10

where

d entrance diameter

D maximum body diameter

X distance from entrance to maximum section

The scoop afterbody consisted of an arbitrary fairing from the scoop maximum section to the exit. (See fig. 1.) The quantity of air flowing through the scoop was controlled by varying the exit area by means of a hinged portion of the fuselage behind the scoop exit (fig. 4). An electric-motor drive was provided in order that the flow quantity could be varied through a given range during each test.

The scoop duct expanded slightly (equivalent to an 8° cone) from the entrance to the scoop maximum section and then contracted to a semicircular section of approximately the same area as the entrance. At this station, pressure measurements to determine inlet-velocity ratio, internal drag, and total pressure were made. The duct remained at approximately constant area back to the hinged exit block. No simulated internal resistance was employed in these tests in order to permit attainment of the high inlet-velocity ratios.

The scoop installation with boundary-layer passage is shown in figure 5. Fuselage undercut, which started at the wing leading-edge station and reached a depth of 5/8 inch at the scoop entrance, provided the frontal area necessary for the boundary-layer entrance. The passage entrance was an annular segment 1/2 inch high with a $\frac{1}{8}$-inch-thick vane separating the main duct and the boundary-layer passage. The passage was divided by a wedge-shape divider and terminated in an exit on each side of the scoop at the maximum section.

An installation with a large amount of fuselage undercut ahead of the scoop was constructed (fig. 6). The fuselage was undercut to the wing lower surface (approximately $1\frac{1}{4}$ in. at the scoop entrance). The resulting boundary-layer-passage entrance was rectangular and was provided with a $\frac{1}{8}$-inch aluminum vane made

detachable to permit variations in entrance height. The passage exits were provided with removable plates by means of which the exit areas and the air-flow quantity in the boundary-layer passage could be varied.

Measurements

Boundary-layer profiles were measured by means of small movable rakes of total-pressure and static-pressure tubes located at various stations on the fuselage surface. At the scoop entrance, the entrance rake was used to determine the boundary-layer profile. The values of boundary-layer thickness were taken as the distance from the model surface to the point beyond which the local total-pressure loss was less than 5 percent of the free-stream dynamic pressure. In order to evaluate the effects of boundary-layer transition occurring near the nose of the fuselage, boundary-layer measurements were made for certain configurations with transition fixed at the 10-percent fuselage station by means of a $\frac{1}{4}$-inch peripheral band of No. 60 carborundum grains shellacked to the surface. Data presented are for natural transition except as otherwise indicated.

Force measurements were made with wing, with wing and basic fuselage, and with wing, fuselage, and scoop in order to evaluate the drag of the various scoop configurations.

The scoop was provided with three longitudinal planes of surface pressure orifices (fig. 3): at the bottom center line; 60° from the bottom center line; and on the side of the scoop, 1/4 inch (at the closest point) from the wing-scoop juncture. Rakes of total-pressure and static-pressure tubes were installed in the scoop entrance (fig. 3) to obtain entrance total-pressure-recovery profiles and within the duct to obtain internal drag and average inlet-velocity ratios. Small rakes of total-pressure and static-pressure tubes were installed in one of the two exits of the boundary-layer duct to obtain average inlet-velocity ratios and internal drag, and at various locations in the boundary-layer inlet to obtain local values of the inlet-velocity ratio. For several tests, wool tufts were attached at various points on and ahead of the scoop in order that the flow conditions might be observed and photographed.

Most of the tests were made at three Mach numbers, 0.30, 0.40, and 0.65, and at three angles of attack, 0°, 3°, and 6°. Certain configurations were tested through a Mach number range from 0.20 to approximately 0.70 and through an angle-of-attack range from 0° to 6°, or to the highest value permitted by model structural limitations. A curve of approximate Reynolds number for the Mach number range of the tests is presented in figure 7.

RESULTS AND DISCUSSION

Boundary-Layer Surveys

Fuselage.- The pressure distributions over the top and bottom surfaces of the fuselage (without scoop) are shown in figure 8. The results of the boundary-layer-thickness survey on the bottom center line of the fuselage are presented in figure 9. The values of boundary-layer thickness are expressed nondimensionally as fractions of the fuselage length. The effects of Reynolds number or Mach number are shown to be small for the range of the tests. The effect of fixing transition near the nose of the fuselage is to increase the boundary-layer thickness by about 45 percent at low angles of attack at the farthest rearward station at which the measurements were made.

Fuselage with original scoop installation.- The pressure distributions on the bottom center line of the fuselage with the scoop are shown in figure 10 for three values of scoop inlet-velocity ratio. Comparison of this figure with figure 8 shows the positive pressure gradient due to the scoop. Figure 10 indicates that the static pressure does not reach the value that might be expected at the scoop entrance at the low inlet-velocity ratios but drops sharply just ahead of the scoop, evidently because of flow separation.

The variations of boundary-layer thickness along the bottom center line of the fuselage with the scoop are shown in figure 11 for scoop inlet-velocity ratios from 0.20 to 0.90. The boundary-layer thickness along the fuselage at the highest inlet-velocity ratio is approximately the same as that shown for the fuselage without the scoop (fig. 9), because only a small

positive pressure gradient exists ahead of the scoop at high inlet-velocity ratios. As the scoop inlet-velocity ratio is decreased, the increase in positive pressure gradient causes abrupt increases in boundary-layer thickness immediately ahead of the scoop entrance until, at $\frac{V_1}{V_o} = 0.20$, the boundary layer almost completely spans the entrance. The thickness of the boundary layer for this condition is about 8 times the normal value. It is apparent that, in advancing into the adverse pressure region ahead of the scoop, the boundary layer has separated the flow and produced a large region in which a substantial loss in total pressure occurs.

The effect of inlet-velocity ratio on boundary-layer thickness at the scoop-entrance center line is shown in figure 12 for both natural and fixed transition through a range of values of Reynolds number. An abrupt increase in δ/l_f is shown to occur when V_1/V_o is decreased to values below 0.6. Reynolds number effects on boundary-layer thickness for the range of these tests are secondary to the effects of inlet-velocity ratio, type of transition, or angle of attack.

Characteristics of Original Scoop Installation

Tuft surveys and internal flow.- In order to determine the type of flow that occurs in the vicinity of the scoop entrance, wool tufts were placed at various locations on the model and photographed. Tuft photographs for the range of inlet-velocity ratios are presented in figure 13.

The corresponding total-pressure-recovery profiles at the scoop entrance and at the duct rake are presented with each photograph. The total-pressure-recovery data are presented in the form

$$1 - \frac{\Delta H}{H_o - p_o} = \frac{H - p_o}{H_o - p_o}$$

This ratio expresses the impact pressure (referenced to free-stream static pressure) available at a particular point as a fraction of the impact pressure available in the free stream. The total-pressure-recovery profiles at the entrance station were measured with a rake

mounted vertically at the center line of the inlet. The profiles in the duct were measured with two radial rakes at a station (fig. 3) where flow conditions had become steady and uniform. The duct profiles therefore are an indication of the average flow losses ahead of that station.

The substantial loss in total pressure that is encountered at the entrance and duct stations at low inlet-velocity ratios is a result of the thickening and separation of the boundary layer ahead of the scoop entrance. The tuft photographs show clearly that the flow is separated, not only in the scoop entrance but also well ahead of the entrance and in the wing-scoop juncture. Increasing the inlet-velocity ratio to a value of 0.6 decreases the total-pressure losses. Above this value, the duct total-pressure losses increase in spite of constantly decreasing boundary-layer thickness at the scoop entrance. The average value of total-pressure-recovery ratio for the highest value of V_1/V_o, from figure 13(f), is 0.8. The losses, as is shown later in results of tests with the boundary layer removed, are a result of increased diffuser losses caused by separation of low-energy boundary-layer air in the diffuser. The tuft photographs show gradual improvement in external flow conditions with increase in inlet-velocity ratio. At $\frac{V_1}{V_o} = 0.90$, all tufts are steady and smooth flow into the scoop takes place.

Typical effects of increasing angle of attack on flow conditions are shown in figure 14 for a medium value of V_1/V_o. The total-pressure loss decreases slightly as the angle of attack increases. (Compare fig. 14 with fig. 13(c).) The tuft photographs also show some improvement in external flow.

The effects of boundary layer are shown to be important through the entire range of inlet-velocity ratios from 0.2 to 0.9. At low inlet-velocity ratios, the boundary layer separates ahead of the scoop entrance; at high inlet-velocity ratios, the flow separates within the diffuser. In all cases, serious losses in total pressure result.

Pressure distributions.- Pressure distributions for three longitudinal planes on the scoop are given in figure 15 for the range of inlet-velocity ratios. At high inlet-velocity ratios, the pressure distributions have low peak negative pressures and no large adverse gradients. Below $\frac{V_1}{V_o} = 0.5$, pressure peaks appear at the scoop lip and continue to rise as the inlet-velocity ratio is decreased to the minimum test value. This change of pressure distribution is to be expected, since a decrease in the scoop inlet-velocity ratio corresponds to an increase in the local angle of attack at the lip.

Critical Mach number.- The critical Mach numbers for the three planes of the scoop are shown in figure 16. These values of M_{cr} were obtained from the measured peak pressures; when necessary, the measured peak was extrapolated beyond the highest test speed by the von Kármán relation (reference 4). The decrease in M_{cr} with decreasing V_1/V_o is a result of the pressure peaks over the scoop lip at low values of V_1/V_o.

The slope of the M_{cr} curves below $\frac{V_1}{V_o} = 0.35$ is less than the slope determined from tests of the same inlet opening with the fuselage boundary layer removed. This effect is due to the flow separation ahead of the inlet previously shown. It is thus indicated that the external flow over the scoop can be seriously affected by the action of the fuselage boundary layer ahead of the scoop. The values of M_{cr} shown for inlet-velocity ratios below $\frac{V_1}{V_o} = 0.6$ have no practical application because the external flow in this range is seriously separated and the drag has already become excessive. The critical speed is lowest for the wing-scoop juncture and highest for the scoop bottom center line for all values of V_1/V_o. Measurement of wing peak negative pressures at several spanwise stations near the scoop installation showed no change in the critical Mach number of the wing due to addition of the scoop. The critical Mach number for the scoop, on the other hand, is shown by figure 16 to be affected to an important extent by the flow field of the wing. This result

exemplifies the adverse effect on critical speed that is encountered when a scoop is located in the superstream-velocity field of a body.

Drag.- Figure 17 shows the drag characteristics of the wing, the wing and streamline fuselage, and the wing, fuselage, and original scoop installation at the design angle of attack of 0°. Drag-coefficient curves for the scoop installation are given for a low, a medium, and a high scoop inlet-velocity ratio. The drag of the model with the scoop installation includes internal drag and the drag of the hinged exit-control block. These data show the drag characteristics of the basic model and the changes that occur with variations in scoop inlet-velocity ratio. The large increase in drag that occurs as V_1/V_o is decreased (fig. 17) is a result of the flow separation.

Characteristics of Scoop with Boundary-Layer Passage

The data from tests of the scoop without boundary-layer passage clearly indicate the necessity of providing a means for handling the fuselage boundary layer in the vicinity of the scoop entrance. For determining the necessary dimensions of the boundary-layer inlet, figure 11 gives a pessimistic indication of the thickness of the layer that should be removed for a scoop operating at low inlet-velocity ratios. On the other hand, it was presumed that removal of the normal thickness of boundary layer at a relatively high inlet-velocity ratio might largely eliminate boundary-layer separation or growth.

The modified scoop installation was provided with a boundary-layer passage having an entrance area of 2.5 square inches and a height of 1/2 inch (about twice the normal boundary-layer thickness at this station). The scoop duct entrance was the same as for the original scoop. In order to provide frontal area for the boundary-layer passage, the fuselage was partially undercut. (See fig. 5.) The passage exits were located near the wing trailing edge at the scoop maximum section where the surface pressure coefficient was of the order of -0.1.

Scoop characteristics are presented in detail for a boundary-layer-passage inlet-velocity ratio of approximately 0.5, which was found to be adequate; the effect of passage inlet-velocity ratio and other variables are discussed later in separate sections.

Tuft surveys and internal flow.- Tuft photographs and total-pressure-recovery profiles are shown for the scoop with the boundary-layer passage in figure 18. No loss in total pressure at the entrance is encountered for the entire range of scoop inlet-velocity ratios, and no measurable loss in total pressure at the duct station occurs until high inlet-velocity ratios are reached. The losses at this condition are approximately one-half those encountered in the scoop without the boundary-layer passage (fig. 13). The tuft photographs show neither irregular nor separated flow for the entire range of scoop inlet-velocity ratios. The necessarily divergent flow ahead of the scoop entrance is evident at low inlet-velocity ratios, but virtually no unsteady flow exists.

Pressure distributions.- The pressure distributions over the scoop with the boundary-layer passage are given in figure 19 for angles of attack of 0° and 3°. The shapes of the pressure distributions and the changes that occur with changes in inlet-velocity ratio are similar to those shown in figure 15 for the scoop without the boundary-layer passage. The peak negative pressures at the low inlet-velocity ratios are higher, however, because of the prevention of separated flow by the boundary-layer-passage installation.

The pressure-distribution data for the three planes of the scoop show the necessity for designing air scoops as three-dimensional bodies. Several tests of scoop installations on specific airplanes (unpublished) substantiate this indication by showing separation over scoop sides that were essentially flat. The sides of a scoop should be designed with proportions and ordinates similar to those used for the bottom plane.

Critical Mach number.- Figure 20 shows the critical speeds of the scoop with the boundary-layer passage for an angle-of-attack range from 0° to 3°. These data establish this scoop as a high-critical-speed installation. The critical Mach number of the scoop (apart

from the wing-scoop juncture) at $\alpha = 0^\circ$ was 0.75 at an inlet-velocity ratio of 0.6. This value of critical Mach number decreased to 0.67 at an inlet-velocity ratio of 0.4. The slightly lower critical speed in the wing-scoop juncture at high inlet-velocity ratios was due in part to wing interference and in part to the approximately constant inlet-velocity ratio in the boundary-layer passage.

The results of these tests show that high-critical-speed scoops can be derived directly from the ordinates of high-critical-speed three-dimensional nose inlets. The derivation of scoop profiles on this basis appears promising and should be considered in future investigations directed toward the development of high-critical-speed scoops. A comparison of the critical Mach number characteristics of this scoop with the characteristics of a corresponding three-dimensional nose inlet is given in reference 5 along with a discussion of the application of nose-inlet design data to the design of fuselage scoops.

Abrupt decreases in critical Mach number occur when the inlet-velocity ratio is lowered below 0.6. Comparison of figure 20 with figure 16 shows the extent to which the critical-speed characteristics of the scoop were altered by the boundary-layer separation that occurred at low inlet-velocity ratios when no boundary-layer passage was provided. The higher values of M_{cr} obtained at low inlet-velocity ratios for the original scoop installation (fig. 16) do not have their usual significance, because the external flow is separated throughout the speed range and the resulting drag has already reached excessive values before the critical Mach number is reached. The critical Mach numbers at the high values of V_1/V_0 are approximately equal for the two installations. These results show that wind-tunnel tests to determine the critical speed of a scoop installation may yield results greatly in error if boundary-layer passages are omitted from the model for simplification. Without boundary-layer passages, entirely different flow conditions are produced, which alter to an important extent the critical-speed, drag, and internal-flow characteristics of the scoop installation.

Effect of boundary-layer-passage inlet-velocity ratio.- The data presented in figures 18 to 20 are for an average $(V_1/V_0)_{BL}$ of approximately 0.5. For all test values of boundary-layer-passage inlet-velocity ratio, the local value of $(V_1/V_0)_{BL}$ at the entrance

center line was found to be between 0.2 and 0.3 higher than the average value. Figure 21 presents tuft photographs for average $(V_1/V_o)_{BL} = 0.2$. Comparison of this figure with figure 18 shows a pronounced change in external flow, particularly at low values of V_1/V_o. The tufts show unsteady flow ahead of the scoop and in the wing-scoop juncture. The total-pressure-recovery profiles (not presented), however, showed no change from those presented in figure 18. Measurement of the recovery profile in the scoop entrance approximately 1/2 inch from the side of the entrance likewise showed no appreciable loss there.

A test was made with the boundary-layer-passage exits sealed. For this condition a local $(V_1/V_o)_{BL}$ of about 0.3 was measured at the entrance center line, an indication that the flow was entering at the center, reversing in the passage, and spilling from the sides of the passage entrance. A small decrease in total-pressure recovery at the duct rake was measured only at high duct inlet-velocity ratios, an indication that a small amount of boundary-layer air was spilling into the main duct for that condition. The satisfactory inlet-velocity ratio maintained in the center of the boundary-layer-passage entrance apparently prevented the boundary layer from spilling into the main duct there; at the sides of the entrance, the air spilled into the lower-pressure region of the wing-scoop juncture rather than into the higher-pressure region of the main duct. Because of this cross flow and spillage, the flow in the main duct was not adversely affected by the decrease in $(V_1/V_o)_{BL}$. The external flow, however, is seriously affected, as is shown by the tuft photographs (fig. 21).

Drag.- The drag data are presented as scoop external-drag coefficients C_{D_F} based on scoop maximum frontal area. The internal drag in the boundary-layer passage, measured at the passage exit, and the internal drag in the scoop duct, measured at the duct rake station (fig. 3), have been deducted from the over-all drag of the scoop. The drag coefficients presented therefore include the internal drag in the rear half of the scoop duct, the exit losses, and the drag of the exit-control block in addition to the scoop drag. The

drag values therefore are somewhat higher than those for other scoop installations, because the scoop configurations as tested did not represent the optimum design from drag considerations.

Drag data are presented in table II for ranges of scoop-duct and boundary-layer-passage inlet-velocity ratios. The reduction in drag made possible by the boundary-layer passage over that of the original installation is evident from the data for the high value of $(V_1/V_o)_{BL}$. For the low value of $(V_1/V_o)_{BL}$, however, the drag is higher than for the original installation. The drag characteristics are shown to be sensitive to changes in $(V_1/V_o)_{BL}$ and indicate that the value of $(V_1/V_o)_{BL}$ must be high enough to prevent separation or spillage from the side of the passage entrance. Increasing $(V_1/V_o)_{BL}$ to above 0.5 might result in further decreases in drag; however, higher passage inlet-velocity ratios were impossible without the use of exit flaps.

Effect of undercutting fuselage.- In order to evaluate the effects of a large amount of undercut ahead of the scoop entrance, the installation was modified as shown in figure 6. Such a modification is of interest as a method of increasing the entrance area of a scoop without increasing the maximum frontal area and to give some information applicable to submerged or partially submerged scoop installations. The amount of undercut at the scoop entrance was approximately $1\frac{1}{4}$ inches, or one-half the original scoop-entrance height. The entrance area of the main duct was increased to 0.0927 square foot, which is a 23-percent increase in area.

Tuft photographs and total-pressure-recovery profiles are shown in figure 22. The pressure-recovery profiles are similar to those presented in figure 18. The tuft photographs, however, show that the flow is unsteady, particularly at the low values of V_1/V_o. In an attempt to improve this condition, the value of $(V_1/V_o)_{BL}$ was increased to 0.7 by means of exit

flaps. Tuft photographs for this condition are shown in figure 23 for four values of V_1/V_o. Some improvement in the flow is apparent, but considerable tuft motion still exists. Observation of these tufts over a period of time showed that the flow ahead of the scoop was alternately rough and smooth. The amount of undercut in this installation is therefore apparently critical. Further undercutting would probably result in failure of the air to follow the fuselage surface.

The drag data for this installation are given in table II(c). The drag coefficient is slightly less than for the partially undercut installation at the high inlet-velocity ratio. At low V_1/V_o, however, the drag is higher, because of the lower value of $(V_1/V_o)_{BL}$ and the slight separation indicated by the tuft photographs.

Effect of varying boundary-layer-passage height.- The height of the passage entrance was reduced from 1/2 inch to 5/16 inch for several tests. (The normal boundary-layer thickness at the scoop-entrance station on the streamline fuselage is approximately 5/16 in.) The total-pressure-recovery profiles for this condition (not presented) show a small loss near the lip, an indication of boundary-layer spillage into the duct. Table II(c) shows a large increase in external drag at low inlet-velocity ratios. Although these tests are not conclusive, it is indicated that use of a boundary-layer-passage height somewhat in excess of the normal boundary-layer thickness at $(V_1/V_o)_{BL} = 0.5$ or less may be advisable, particularly for scoops operating at low or medium inlet-velocity ratios.

CONCLUDING REMARKS

A large air scoop designed for high critical speed has been tested on the fuselage of a $\frac{1}{5}$-scale fighter-type airplane. The critical Mach number of the scoop (apart from the wing-scoop juncture) was 0.75 at an inlet-velocity ratio of 0.6. This value of critical Mach number decreased to 0.67 at an inlet-velocity ratio of 0.4. A slightly lower critical speed was

attained in the wing-scoop juncture, largely because of the flow field of the wing. Pressure measurements over several planes of the scoop indicated that the sides of a scoop should be designed with proportions and ordinates similar to those used for the bottom plane.

The results of these tests showed that high-critical-speed scoops can be derived directly from the ordinates of high-critical-speed three-dimensional nose inlets. The derivation of scoop profiles on this basis appears promising and should be considered in future investigations directed toward the development of high-critical-speed scoops.

The positive pressure gradient ahead of the scoop at low inlet-velocity ratios caused the fuselage boundary layer to separate and to attain a thickness at the scoop entrance approximately 8 times the normal boundary-layer thickness. At inlet-velocity ratios approaching unity, the boundary layer at the scoop entrance was of the same thickness as that on the fuselage without a scoop.

The effects of boundary layer on scoop characteristics were important at all inlet-velocity ratios. At low values of inlet-velocity ratio, significant losses in total pressure available in the duct and large increases in external drag were found to occur as a result of flow separation ahead of the scoop entrance. At high inlet-velocity ratios, the boundary-layer air induced separation in the scoop diffuser, which caused equally significant total-pressure losses. The critical Mach number of the scoop installation was altered by the external separation occurring at low inlet-velocity ratios.

A boundary-layer passage of height about twice the normal fuselage boundary-layer thickness eliminated the internal losses in the scoop duct due to the boundary layer. The inlet-velocity ratio in the boundary-layer passage was indicated to be of importance for, with increases in boundary-layer-passage inlet-velocity ratio, the external drag of the installation decreased. A boundary-layer-passage inlet-velocity ratio of 0.5 was found to give a substantial reduction in drag and to provide (as shown by tuft surveys) smooth external flow; however, additional improvement might be realized at higher passage inlet-velocity ratios.

Undercutting the fuselage ahead of the scoop by one-half the original scoop-entrance height, as a means of increasing the scoop-entrance area, was indicated to be critical from consideration of fuselage flow separation.

Langley Memorial Aeronautical Laboratory
National Advisory Committee for Aeronautics
Langley Field, Va.

REFERENCES

1. Abbott, Ira H.: Fuselage-Drag Tests in the Variable-Density Wind Tunnel: Streamline Bodies of Revolution, Fineness Ratio of 5. NACA TN No. 614, 1937.

2. Abbott, Ira H., von Doenhoff, Albert E., and Stivers, Louis S., Jr.: Summary of Airfoil Data. NACA ACR No. L5C05, 1945.

3. Becker, John V.: Wind-Tunnel Tests of Air Inlet and Outlet Openings on a Streamline Body. NACA ACR, Nov. 1940.

4. von Kármán, Th.: Compressibility Effects in Aerodynamics. Jour. Aero. Sci., vol. 8, no. 9, July 1941, pp. 337-356.

5. Baals, Donald D., Smith, Norman F., and Wright, John B.: The Development and Application of High-Critical-Speed Nose Inlets. NACA ACR No. L5F30a, 1945.

TABLE I.- MODEL ORDINATES

[All measurements in in. See figs. 1 and 3.]

Fuselage			Wing				Scoop and duct			
			Upper surface		Lower surface					
x_f	y_f	w_f	x_w	y_U	x_w	y_L	x_s	y_c	r_s	r_d
0	0	0	0	0	0	0	0	6.48	2.54	2.50
.75	1.01	.96	.097	.253	.123	-.238	.2	↑	2.76	2.52
1.00	1.24	1.17	.150	.306	.180	-.286	.6		2.94	2.57
1.25	1.45	1.35	.258	.388	.292	-.357	1.0		3.08	2.60
2.50	2.27	2.03	.531	.529	.569	-.476	2.0		3.35	2.69
5.00	3.36	2.89	1.079	.727	1.121	-.636	3.0		3.55	2.76
7.00	4.04	3.32	1.628	.883	1.672	-.760	4.0		3.69	2.83
9.00	4.61	3.61	2.178	1.014	2.222	-.863	5.0		3.80	2.89
11.00	5.05	3.80	3.279	1.218	3.321	-1.020	6.0		3.90	2.93
15.00	5.64	3.97	4.381	1.373	4.419	-1.139	6.8	Straight line	3.94	2.96
16.50	5.81	4.00	5.484	1.494	5.517	-1.229	7.0		3.95	2.96
18.00	5.91	↑	6.587	1.584	6.613	-1.296	8.0	↓	3.98	2.96
21.00	6.20		7.690	1.649	7.710	-1.342	8.8	6.48	4.00	2.88
22.00	6.26		8.794	1.688	8.806	-1.369	9.0	6.47	4.00	2.86
25.00	6.40		9.897	1.702	9.902	-1.377	9.5	6.45	3.98	2.81
30.00	6.50		11.002	1.691	10.998	-1.367	10.0	6.43	3.96	2.77
32.50	6.50		12.107	1.651	12.093	-1.332	10.5	6.39	3.94	2.74
34.50	6.49		13.213	1.574	13.187	-1.272	11.0	6.34	3.89	2.71
35.20	6.47		14.318	1.443	14.282	-1.167	11.5	6.30	3.86	2.70
38.00	6.40		15.419	1.260	15.361	-1.018	12.0	6.24	3.82	2.70
40.25	6.30		16.517	1.047	16.483	-.843	13.0	6.11	3.74	2.74
42.00	6.19		17.614	.817	17.586	-.655	14.0	5.97	3.66	2.79
44.00	6.06	4.00	18.710	.578	18.690	-.458	15.0	5.83	3.58	2.83
46.00	5.93	3.97	19.806	.345	19.794	-.268	17.0	5.50	3.37	2.87
47.00	5.86	3.95	20.902	.133	20.898	-.097	19.0	5.12	3.13	2.87
50.00	5.60	3.90	22.000	0	22.000	0	20.0	4.90	2.98	2.95
54.50	5.03	3.69								
54.70	5.00	3.68					Scoop-lip radius: 0.04			
55.20	4.92	3.65								
56.50	4.72	3.54								
60.00	4.08	3.21								
65.00	3.16	2.58								
68.00	2.58	2.09								
70.00	2.16	1.76								
72.50	1.63	1.34								
75.00	1.09	.91								
77.50	.53	.46								
78.75	.26	.24								
80.00	0	0								

NATIONAL ADVISORY
COMMITTEE FOR AERONAUTICS

TABLE II.- EXTERNAL-DRAG COEFFICIENTS

FOR SCOOP INSTALLATIONS

[$\alpha = 0^\circ$]

(a) Original scoop; M = 0.40	
V_1/V_o	C_{D_F}
0.20	0.222
.40	.177
.90	.132

(b) Scoop with boundary-layer passage; partially undercut fuselage; M = 0.30			
$(V_1/V_o)_{BL} = 0.5$		$(V_1/V_o)_{BL} = 0.2$	
V_1/V_o	C_{D_F}	V_1/V_o	C_{D_F}
0.22	0.168	0.24	0.260
.35	.145	.47	.194
1.00	.116	.98	.143

(c) Scoop with boundary-layer passage; fully undercut fuselage; M = 0.30			
Passage-entrance height, 1/2 in.; $(V_1/V_o)_{BL} = 0.4$		Passage-entrance height, 5/16 in.; $(V_1/V_o)_{BL} = 0.45$ to 0.3[a]	
V_1/V_o	C_{D_F}	V_1/V_o	C_{D_F}
0.21	0.211	0.19	0.260
.32	.177	.29	.190
.53	.128	.50	.130
.84	.104	.80	.103

[a] $(V_1/V_o)_{BL}$ decreased as V_1/V_o increased.

NATIONAL ADVISORY
COMMITTEE FOR AERONAUTICS

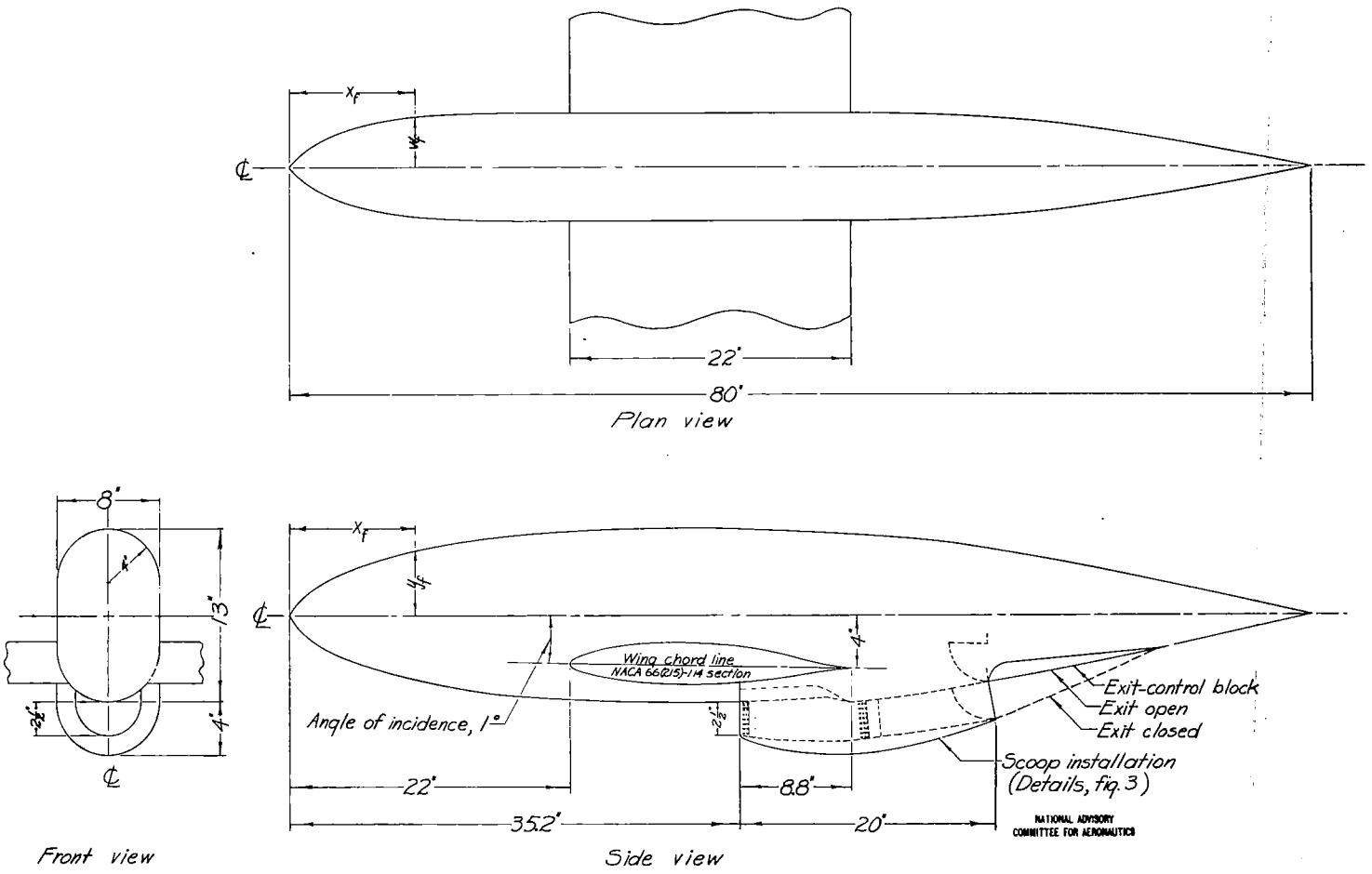

Figure 1.-Model arrangement.

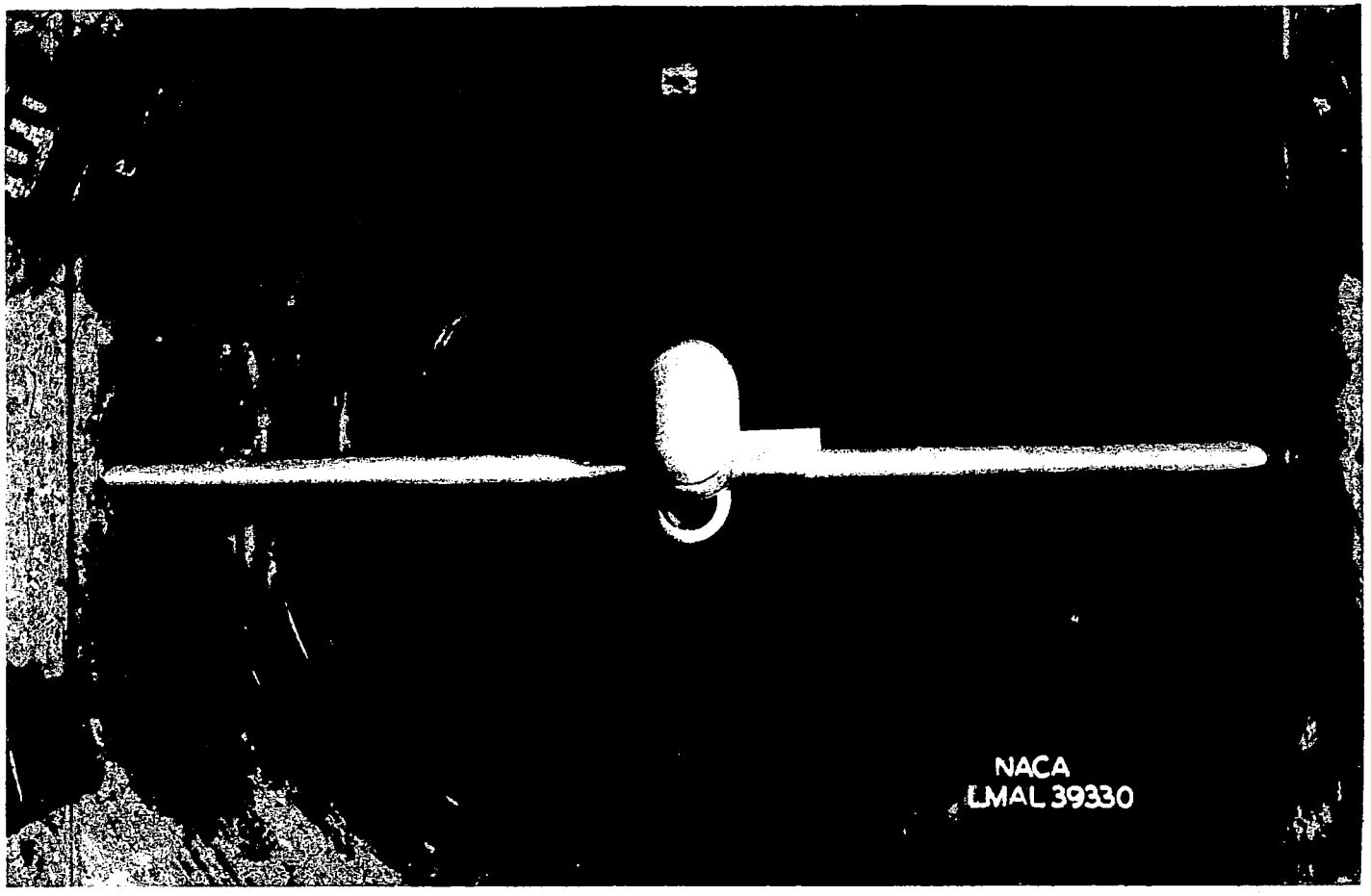

Figure 2.- Installation of model in the Langley 8-foot high-speed tunnel.

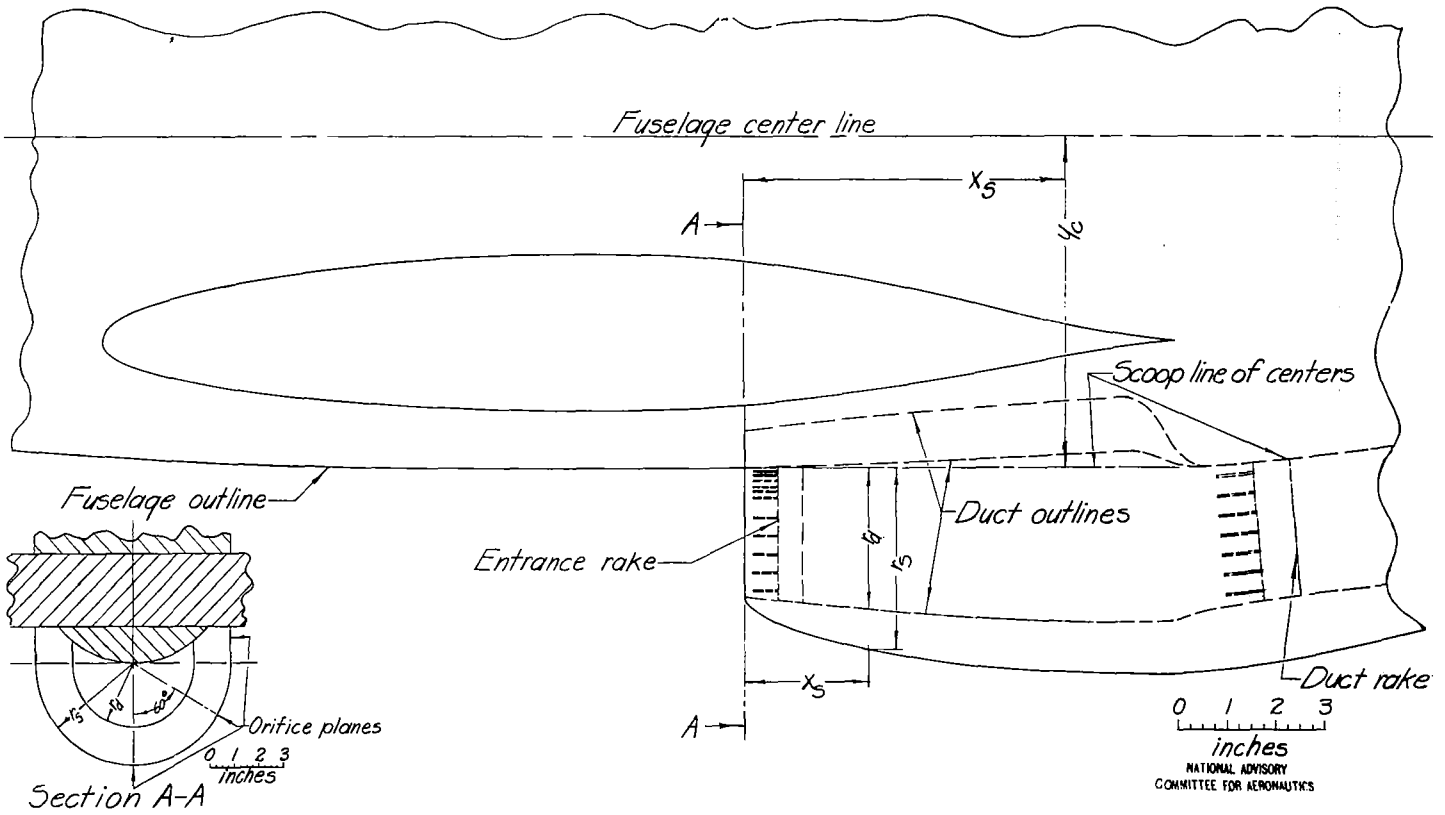

Figure 3.-Details of original scoop installation.

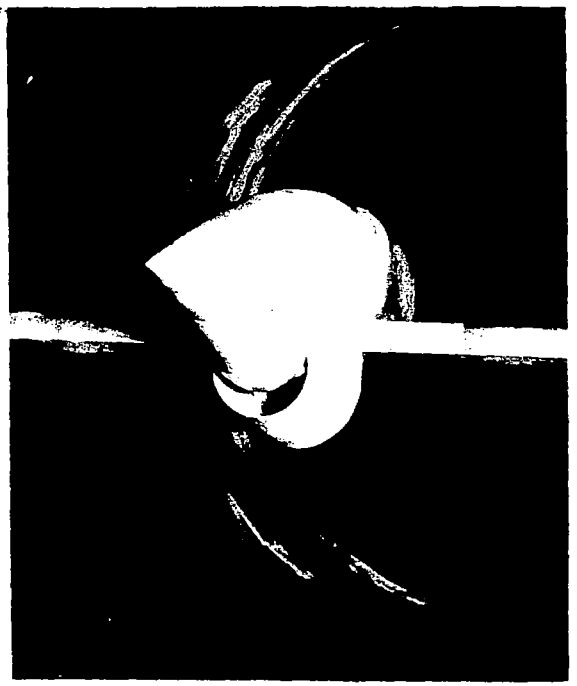

(a) Half-closed position.

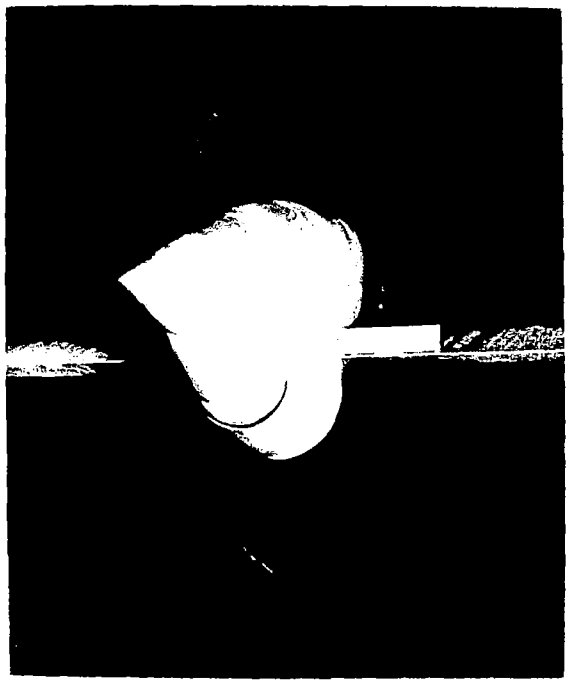

(b) Fully closed position.

Figure 4.- Details of exit-control block.

NATIONAL ADVISORY
COMMITTEE FOR AERONAUTICS

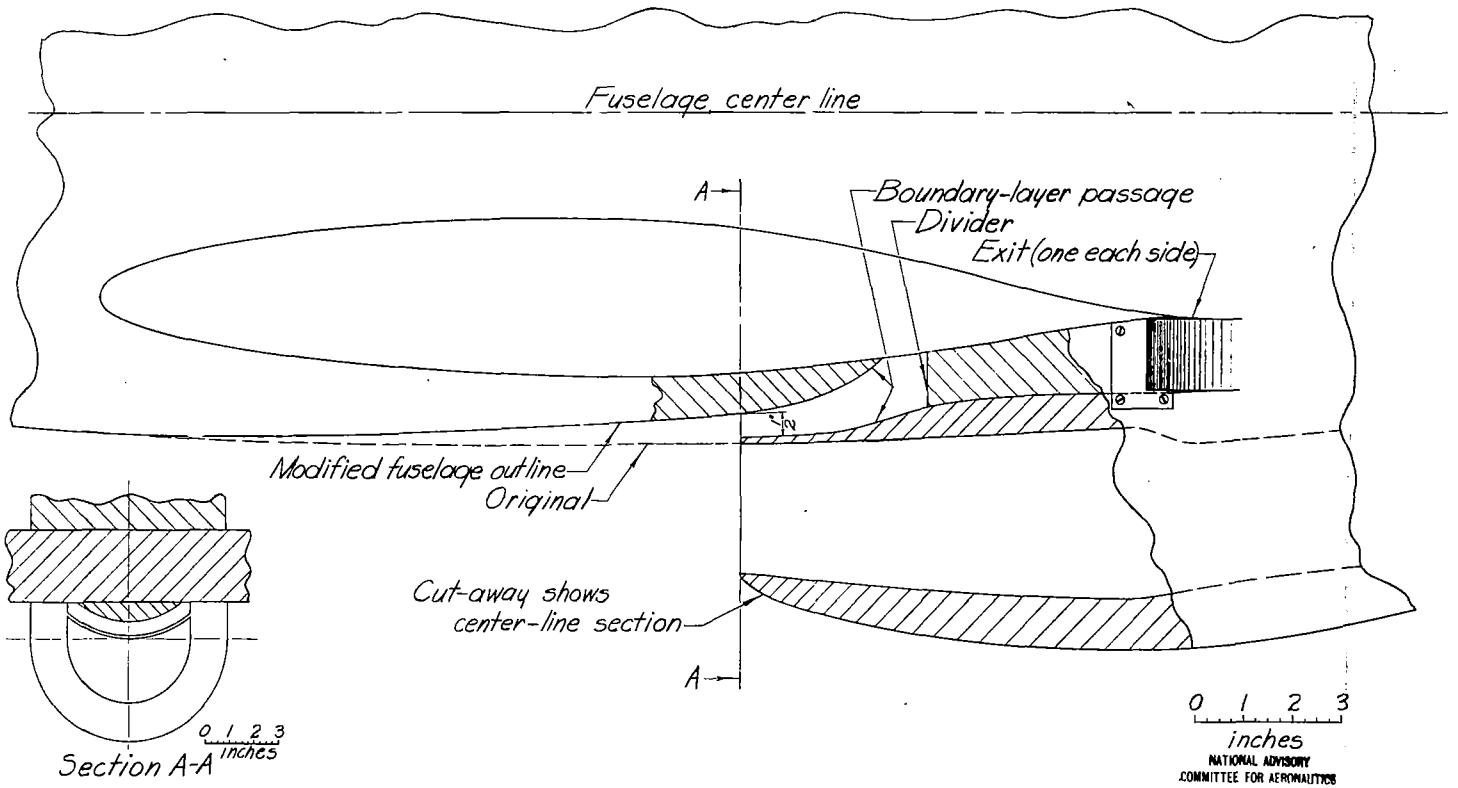

Figure 5.-Scoop with boundary-layer passage and partially undercut fuselage.

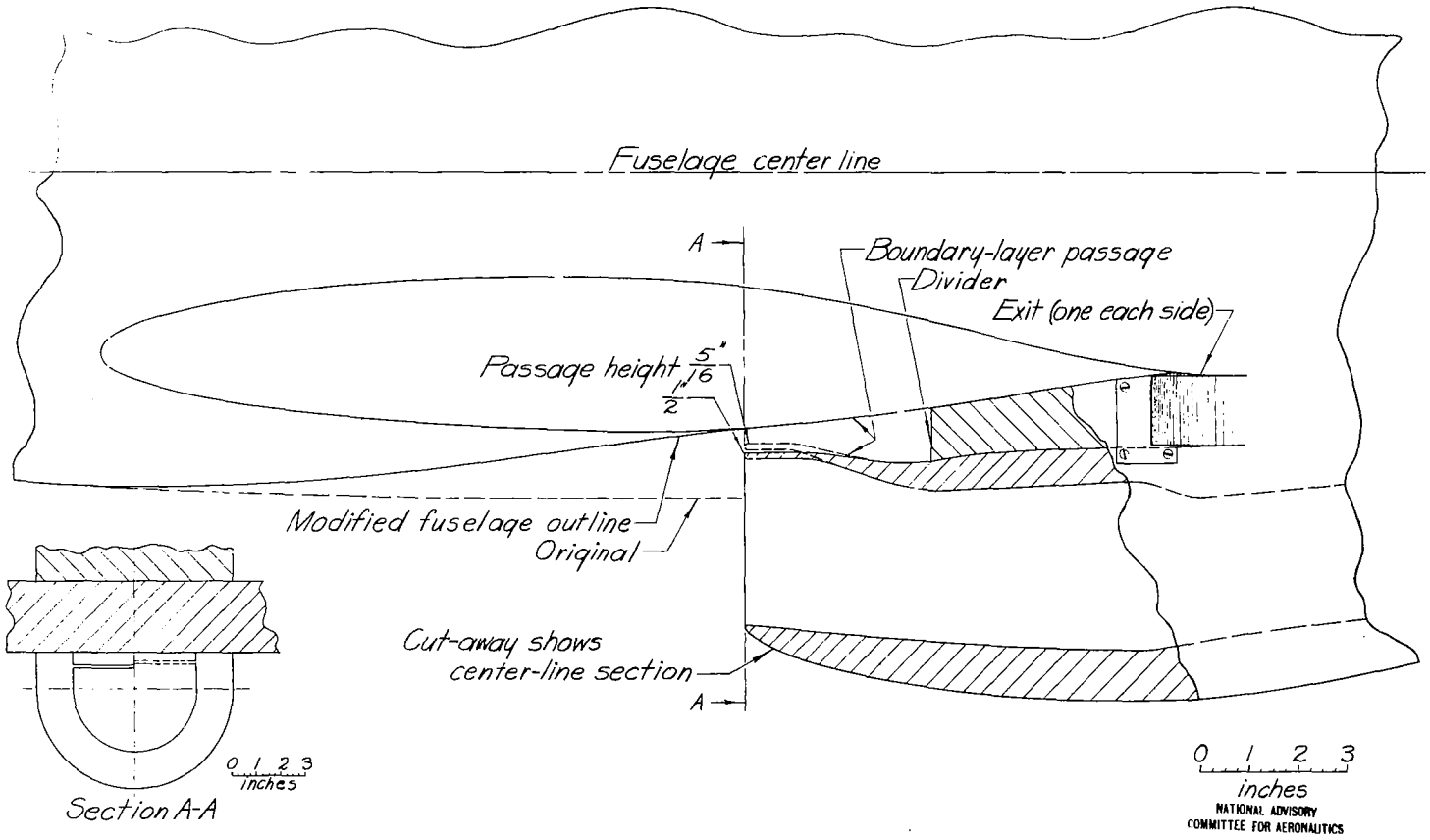

Figure 6.-Scoop with boundary-layer passage and fully undercut fuselage.

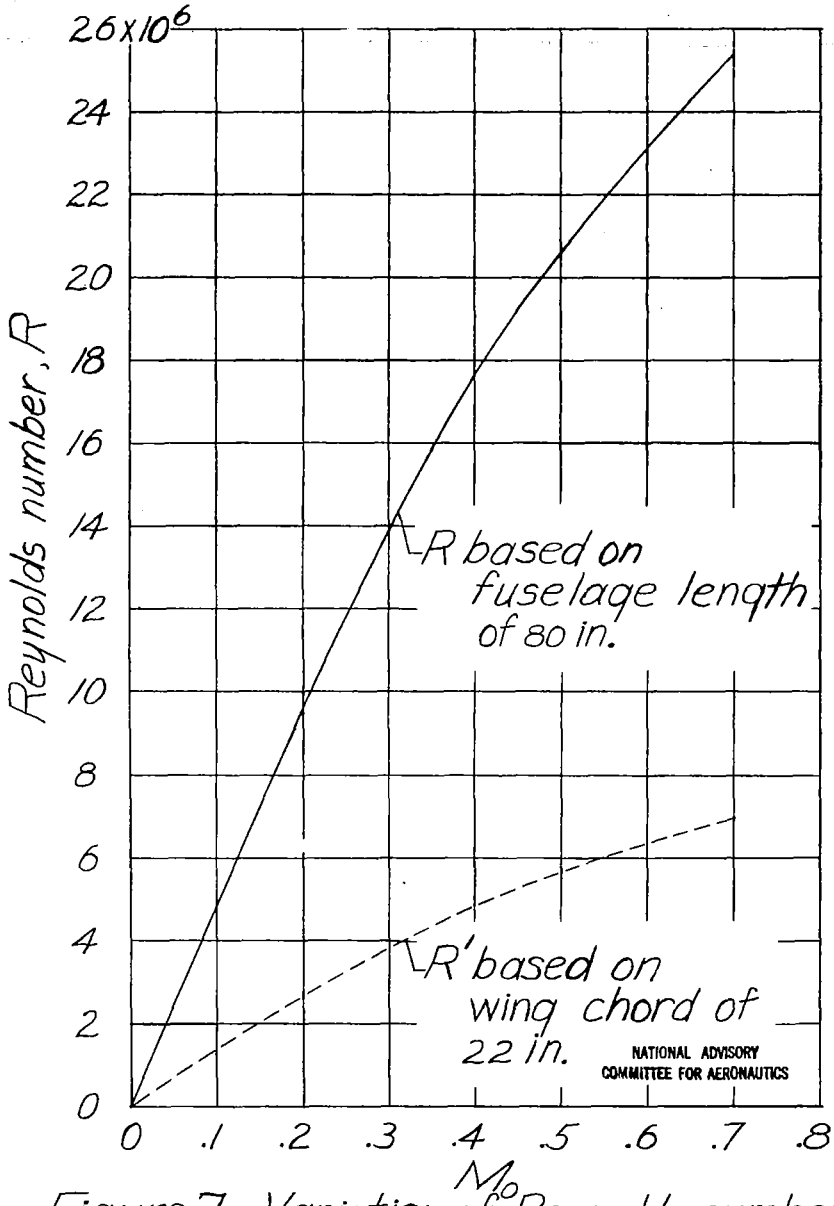

Figure 7.- Variation of Reynolds number (approx.) with Mach number in the Langley 8-foot high-speed tunnel.

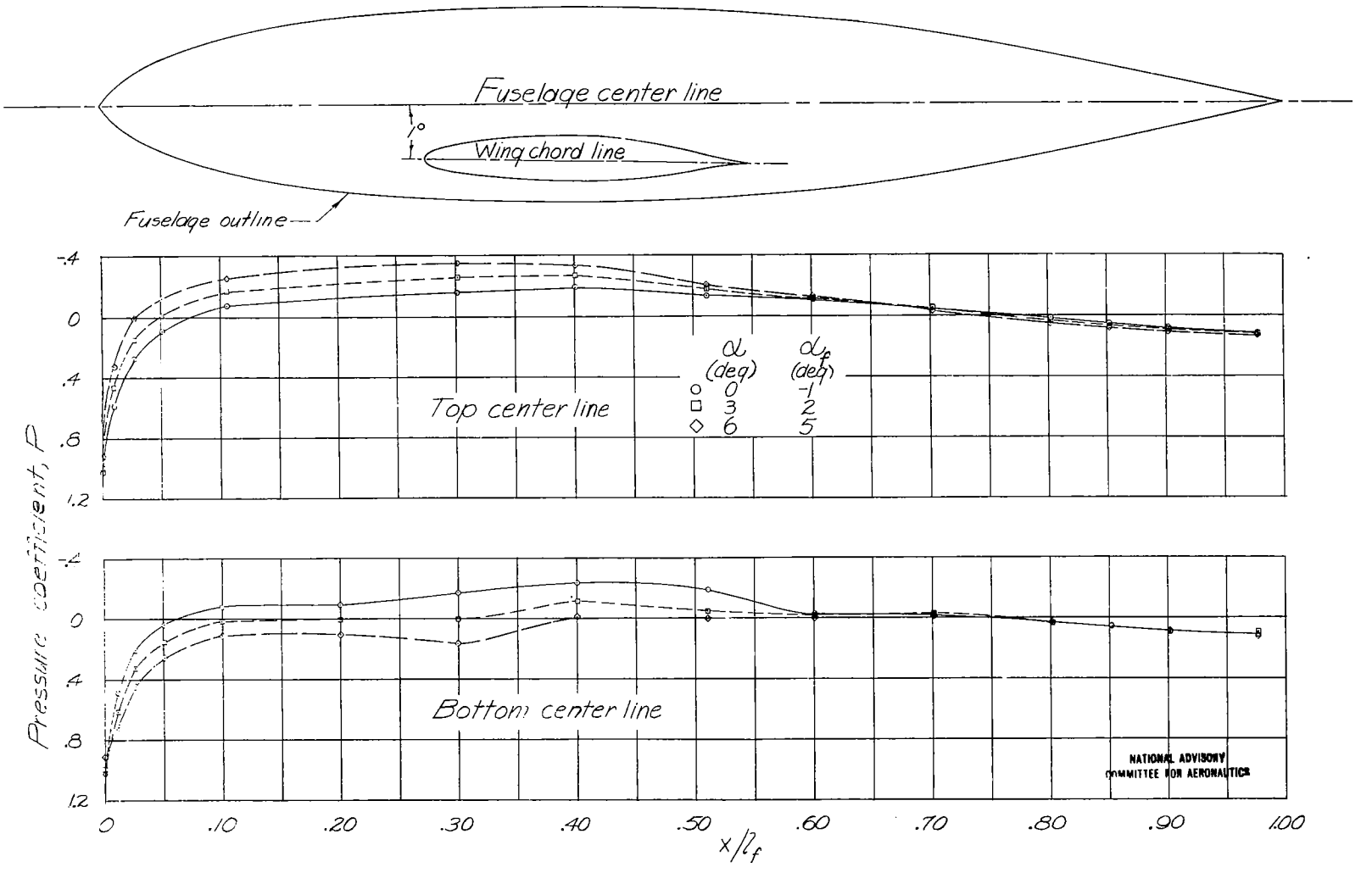

Figure 8.-Pressure distributions on top and bottom center line of fuselage without scoop. M_0=0.30.

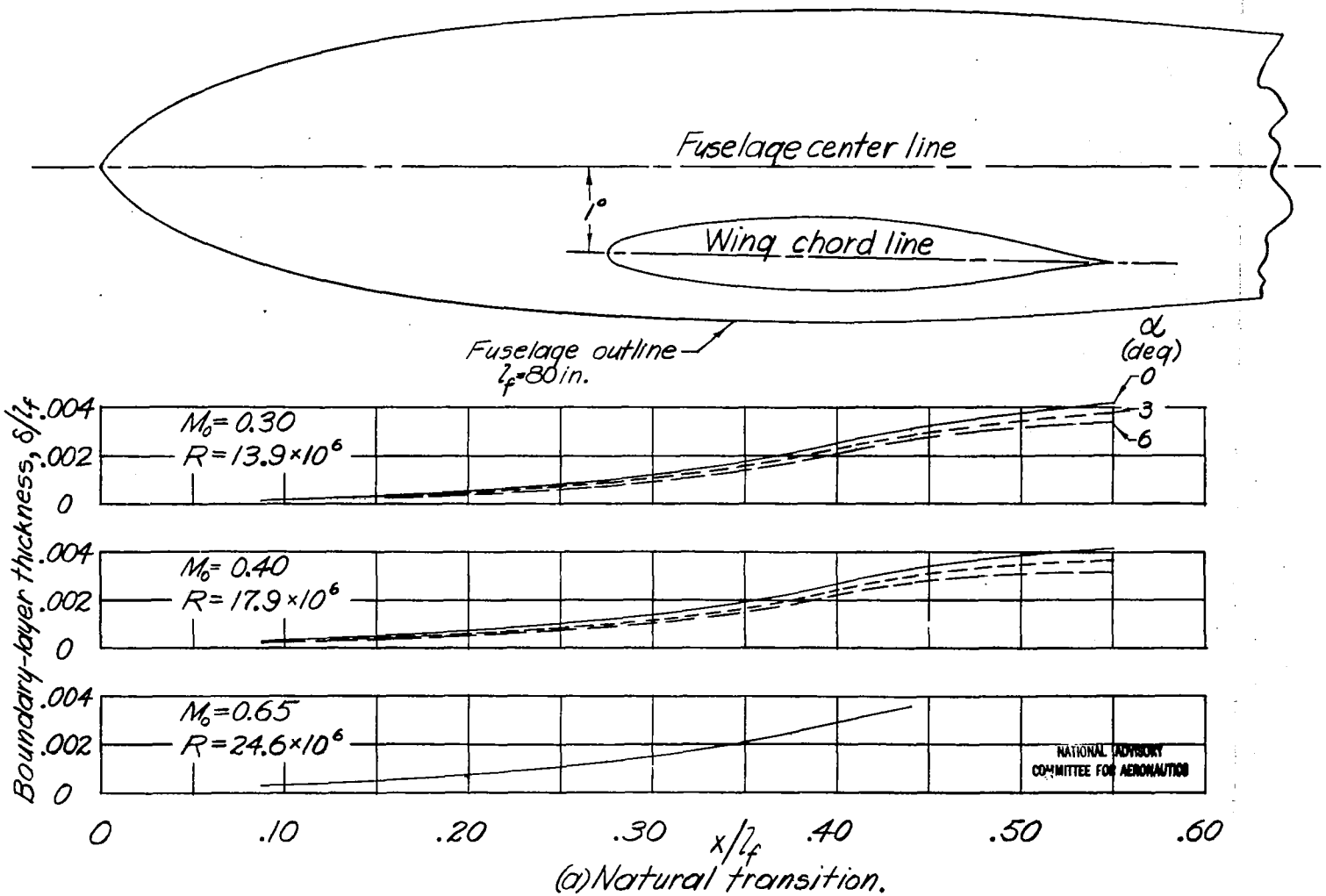

(a) Natural transition.

Figure 9.-Boundary-layer thickness on bottom center line of fuselage.

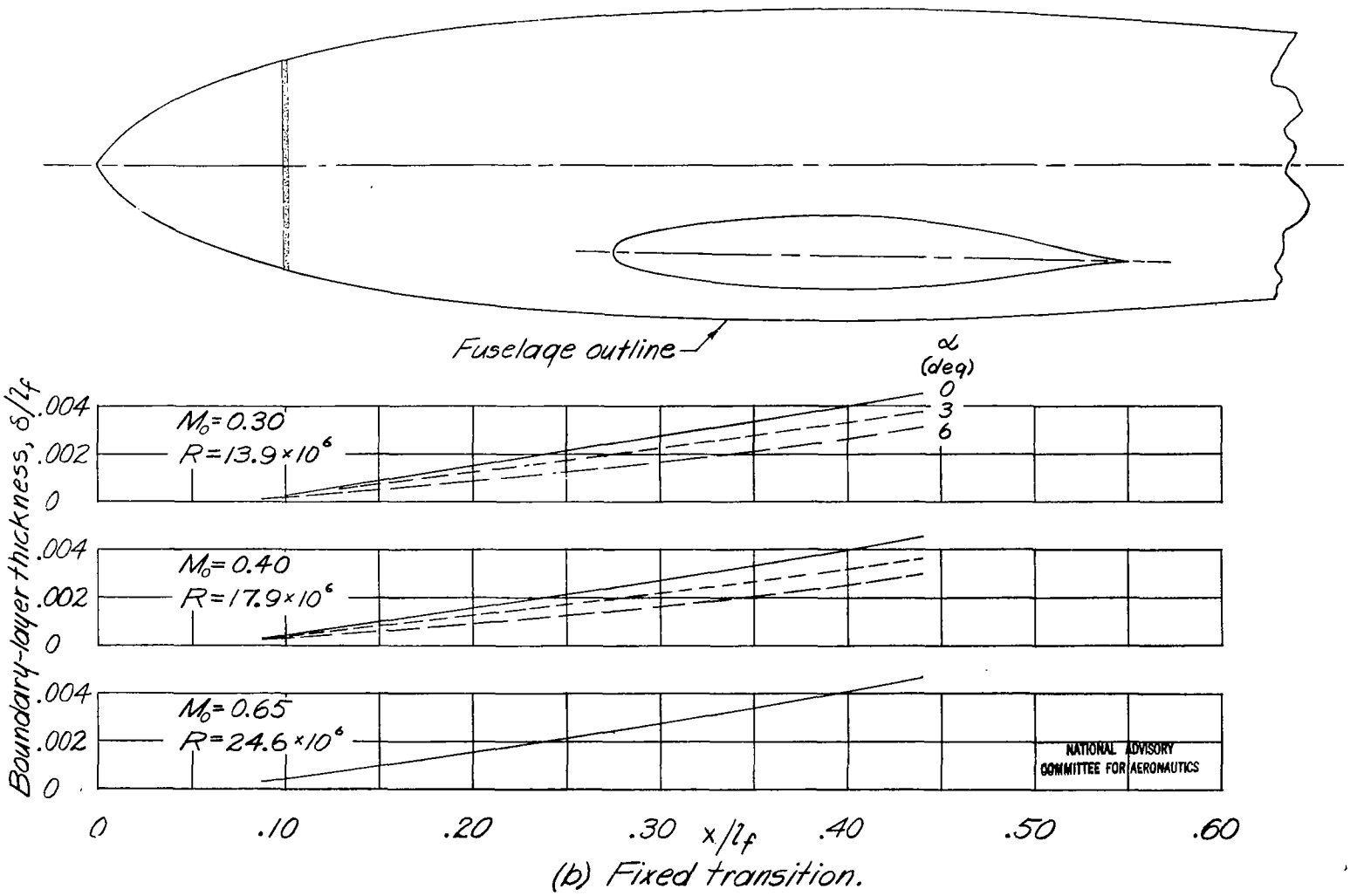

(b) Fixed transition.

Figure 9.-Concluded.

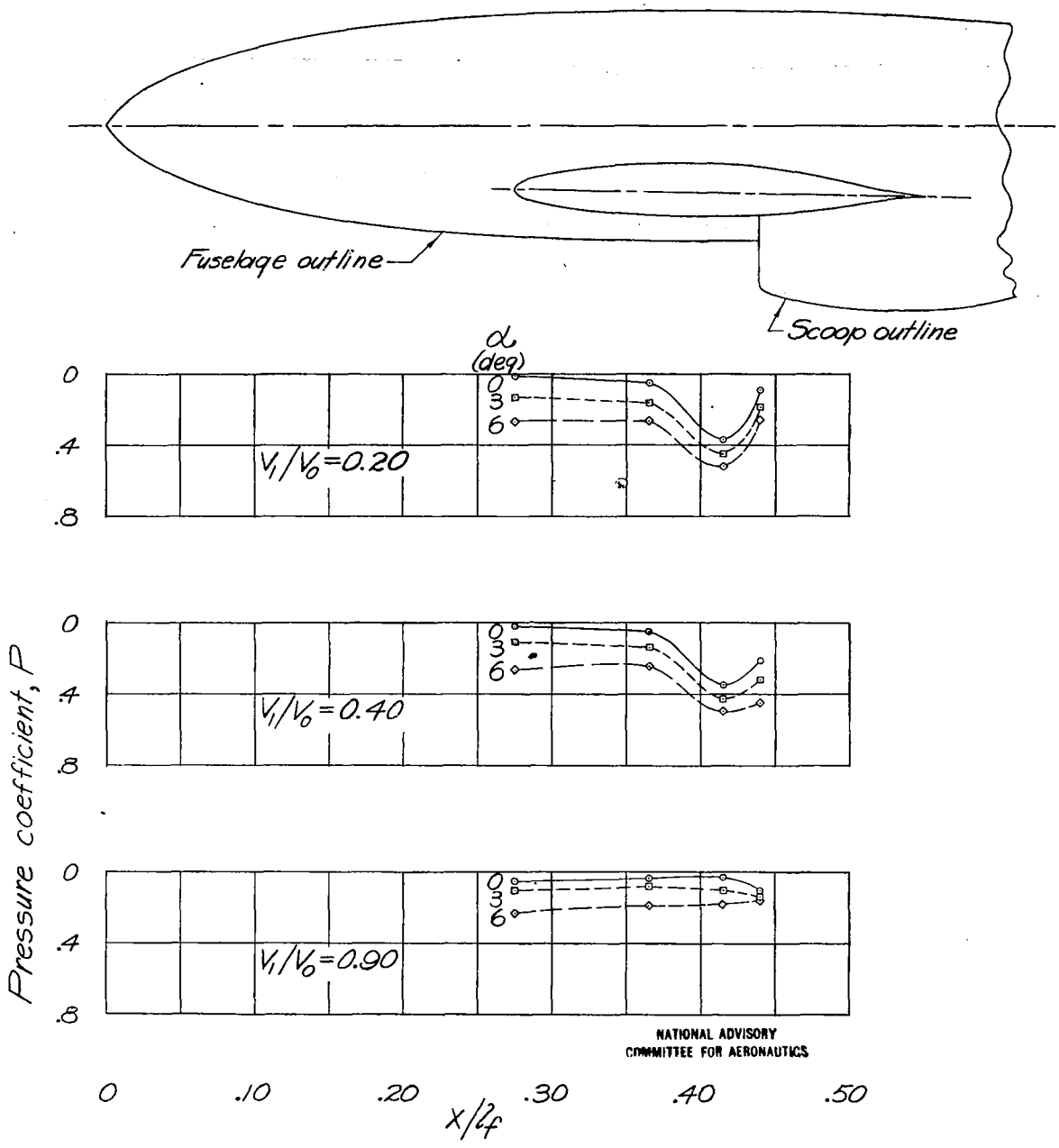

Figure 10.—Pressure distributions on bottom center line of fuselage ahead of original scoop installation. $M_0=0.30$.

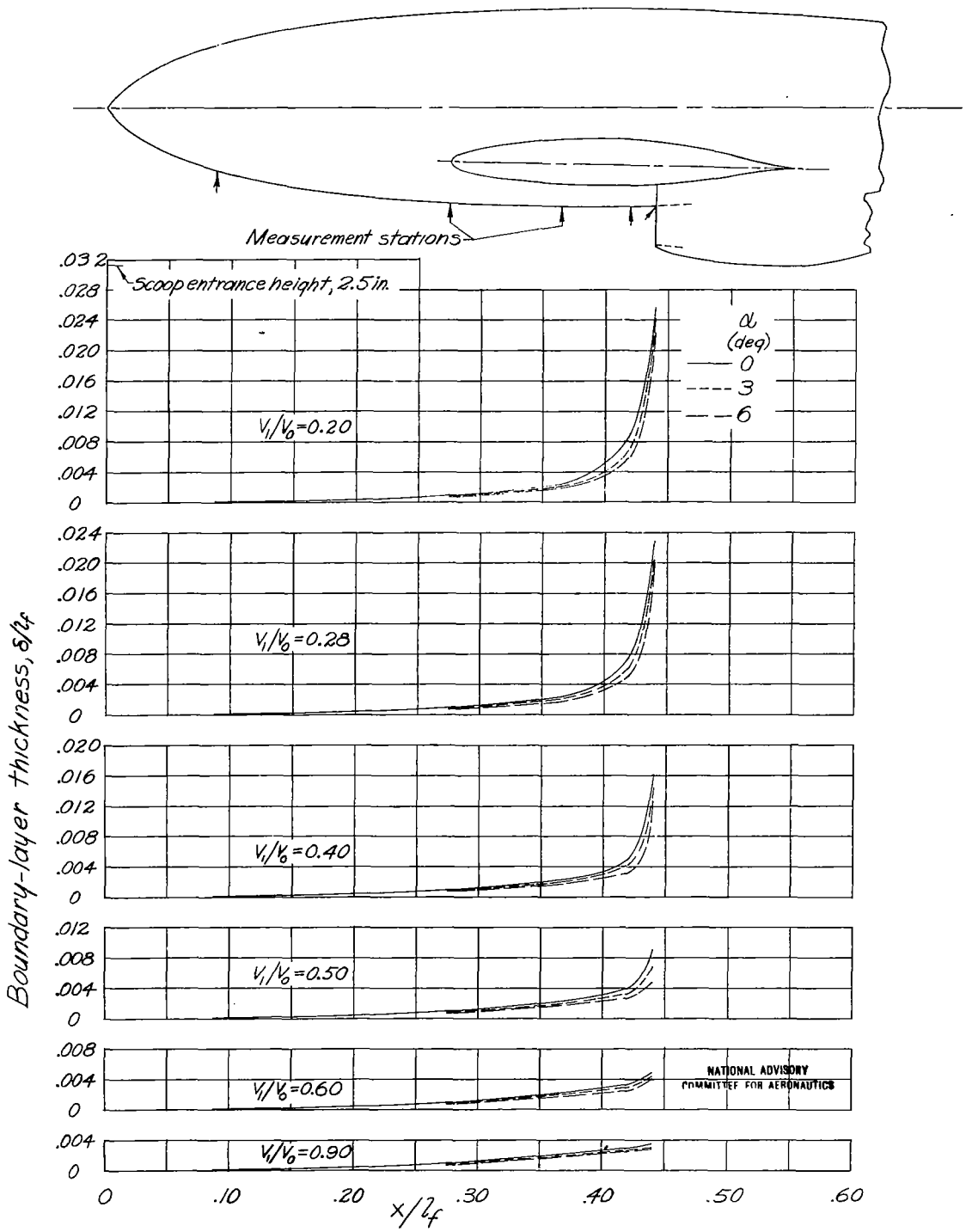

Figure 11.- Boundary-layer thickness on bottom center line of fuselage with original scoop installation. Natural transition; M_0=0.30; R=13.9×10⁶.

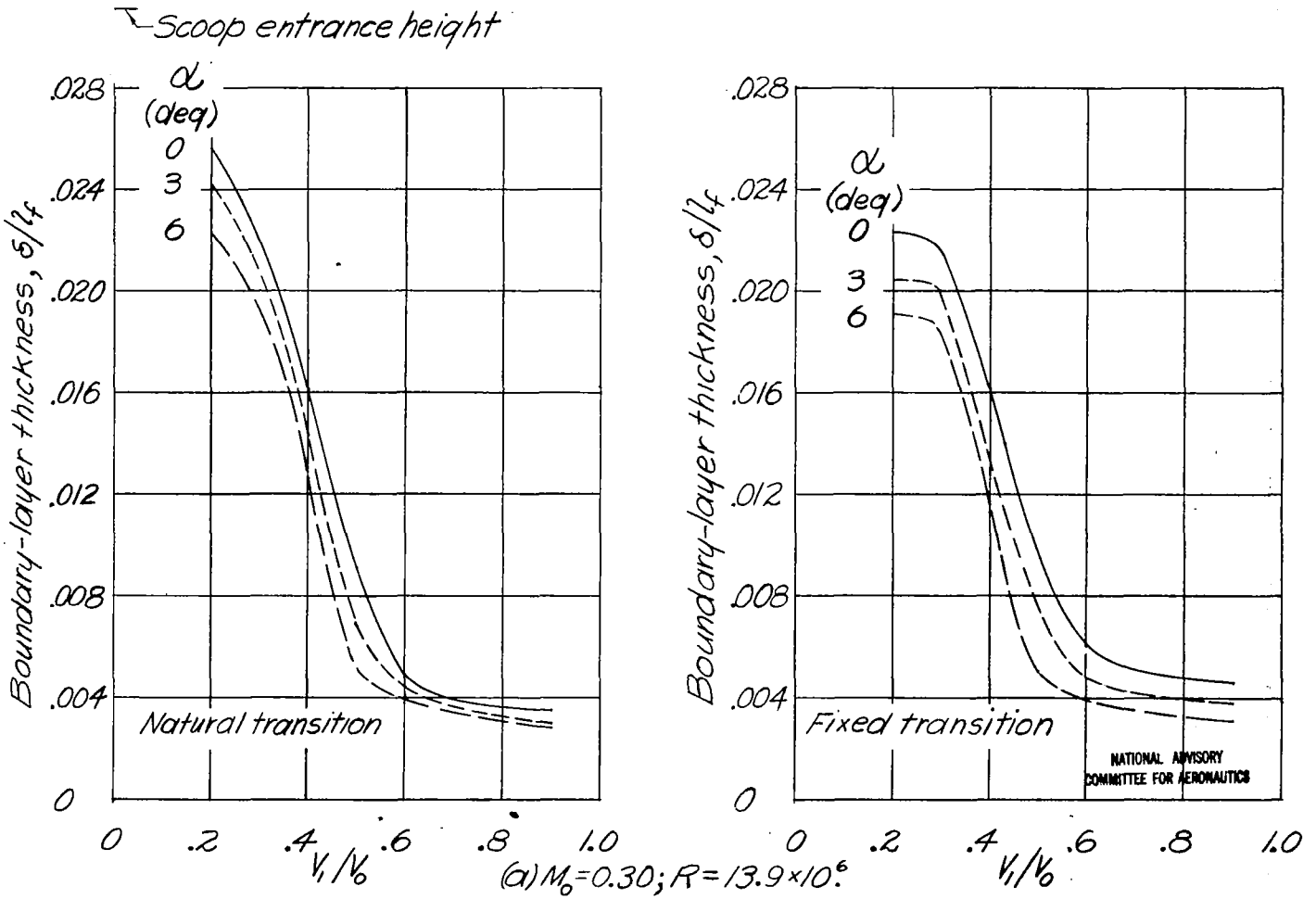

(a) $M_0 = 0.30$; $R = 13.9 \times 10^6$.

Figure 12.- Boundary-layer thickness at center line of entrance of original scoop.

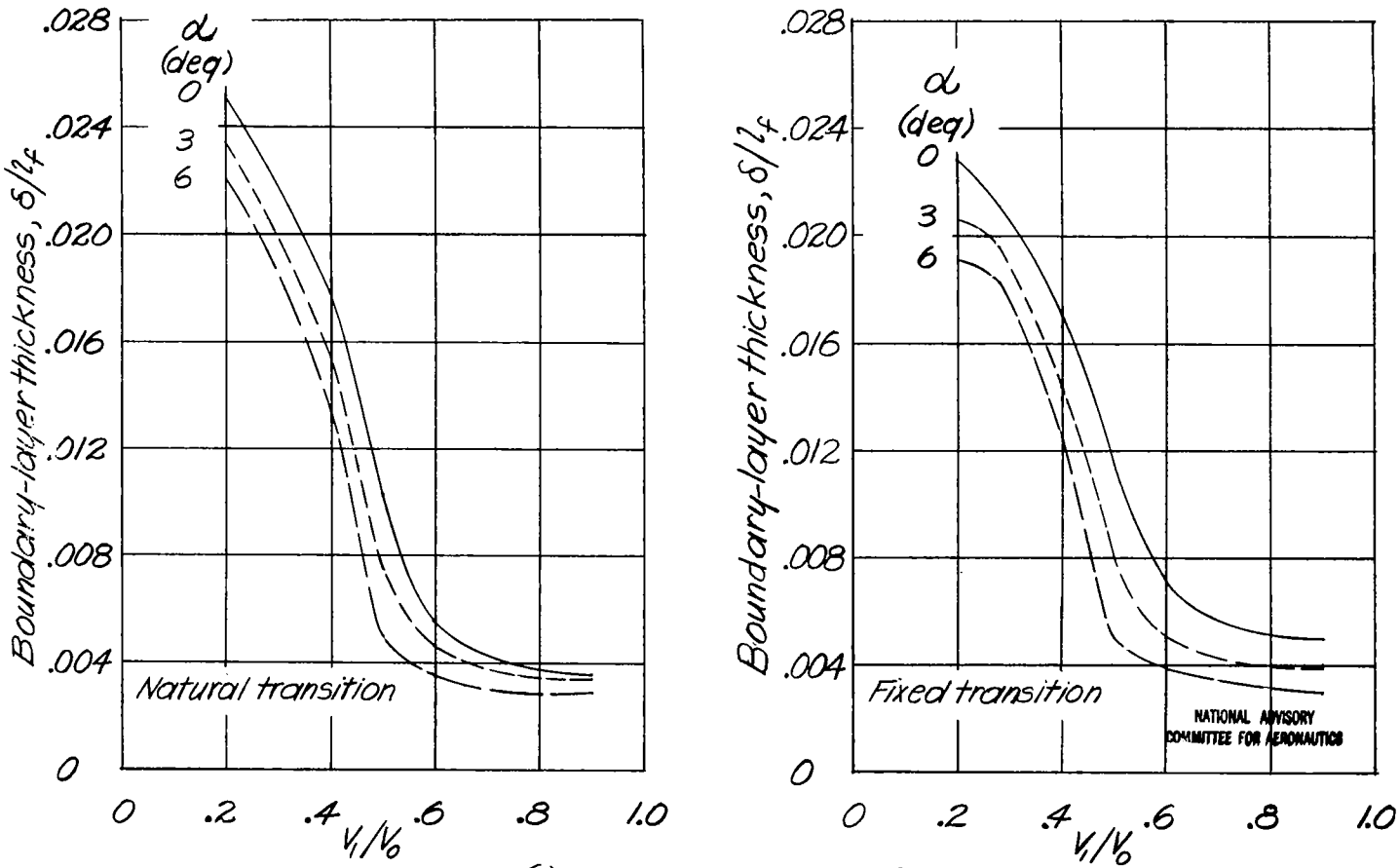

(b) $M_0 = 0.40$; $R = 17.9 \times 10^6$

Figure 12.- Continued.

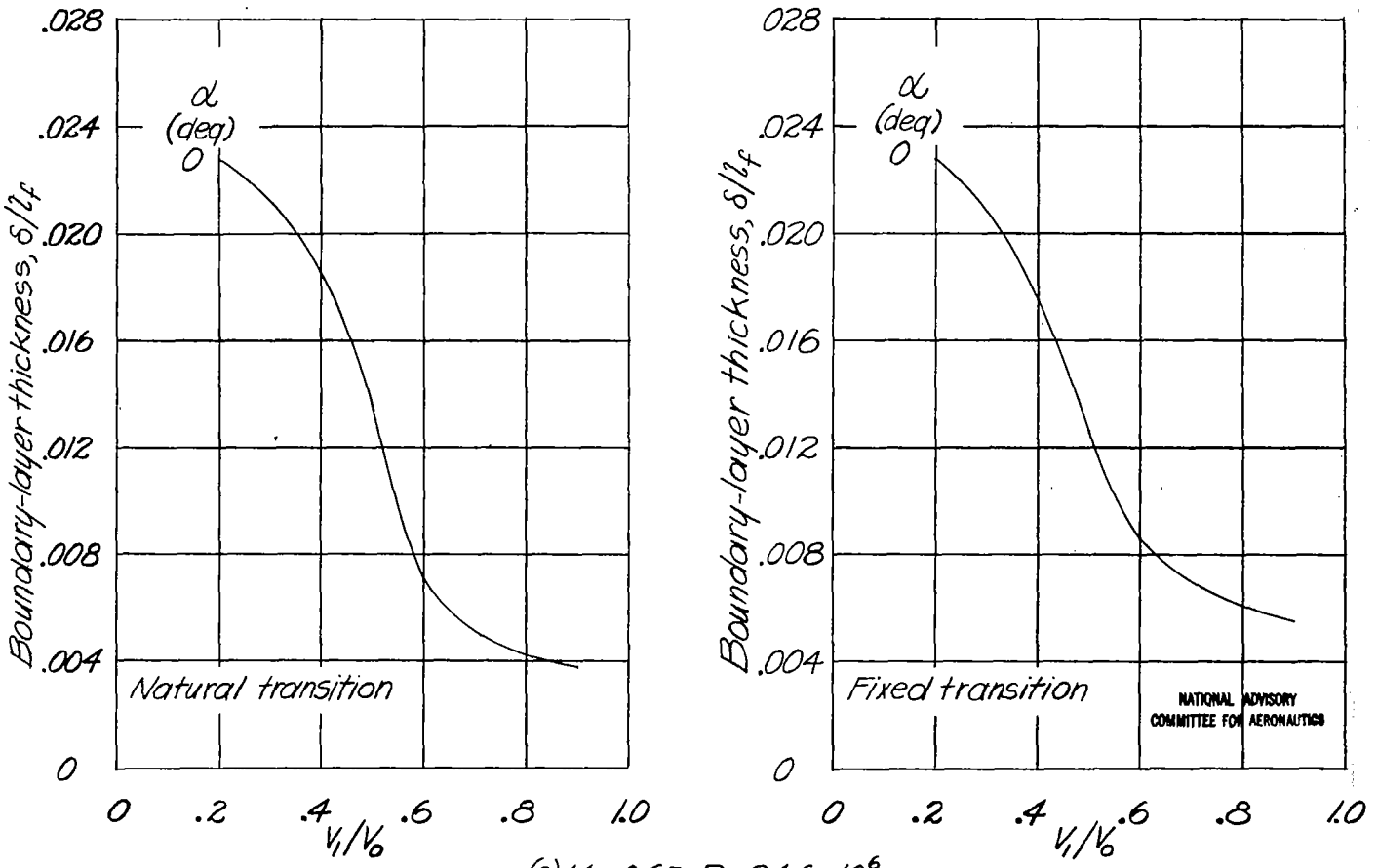

(c) $M_0 = 0.65$; $R = 24.6 \times 10^6$

Figure 12.—Concluded.

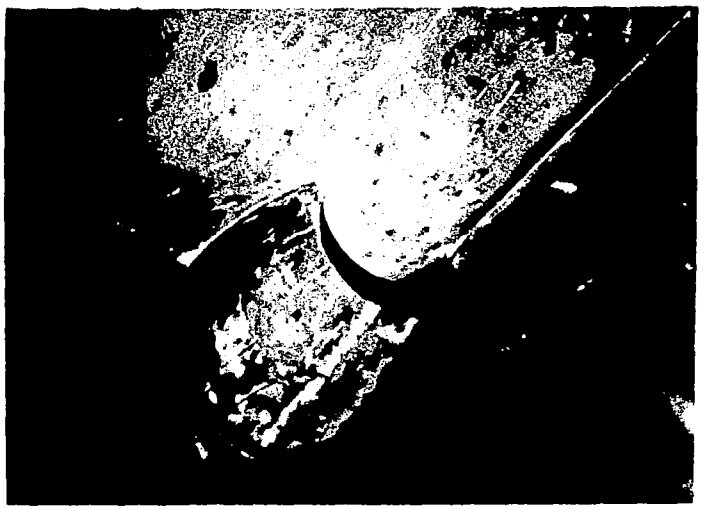

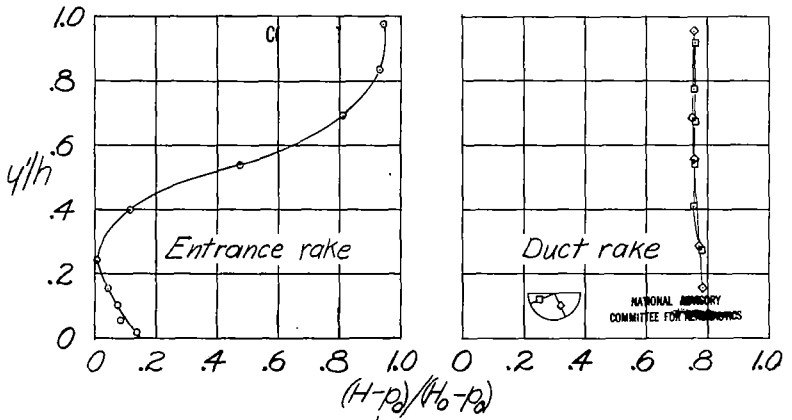

(a) $V_1/V_0 = 0.20$.

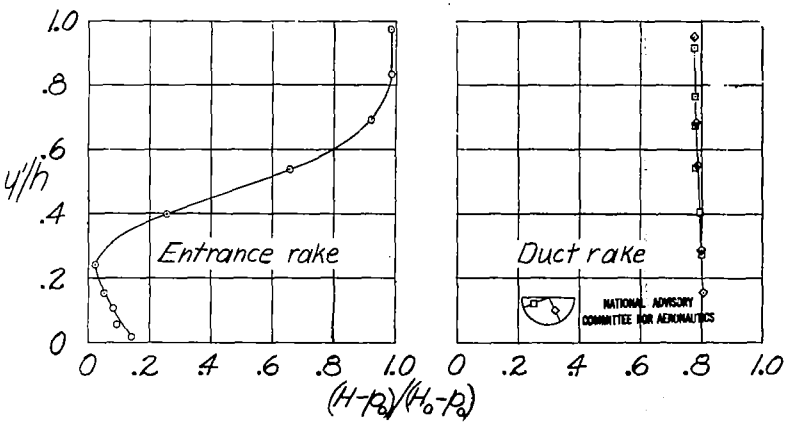

(b) $V_1/V_0 = 0.28$.

Figure 13.- Tuft photographs and total-pressure-recovery profiles for original scoop for various inlet-velocity ratios. $\iota = 0^\circ$; $M_0 = 0.40$.

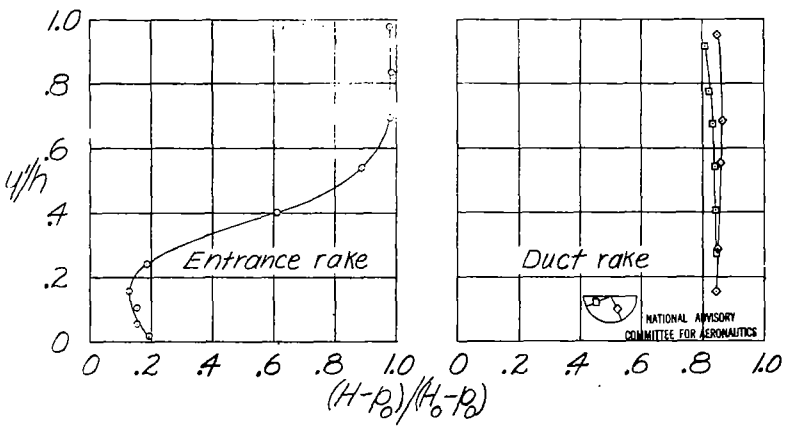

(c) $V_1/V_0 = 0.40$.

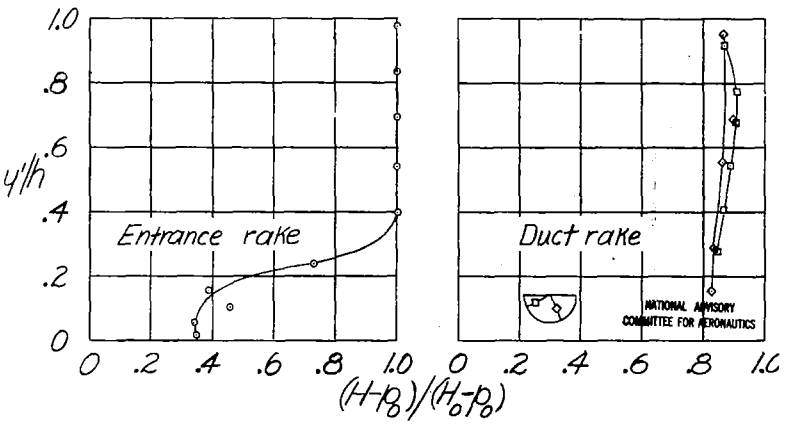

(d) $V_1/V_0 = 0.50$.

Figure 13.- Continued.

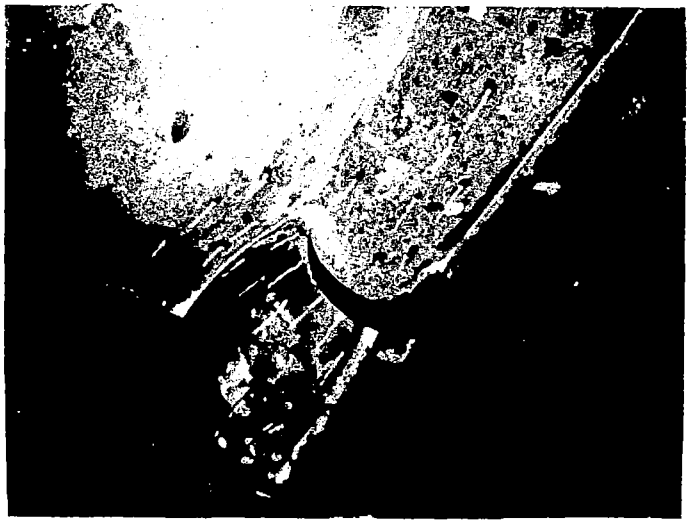

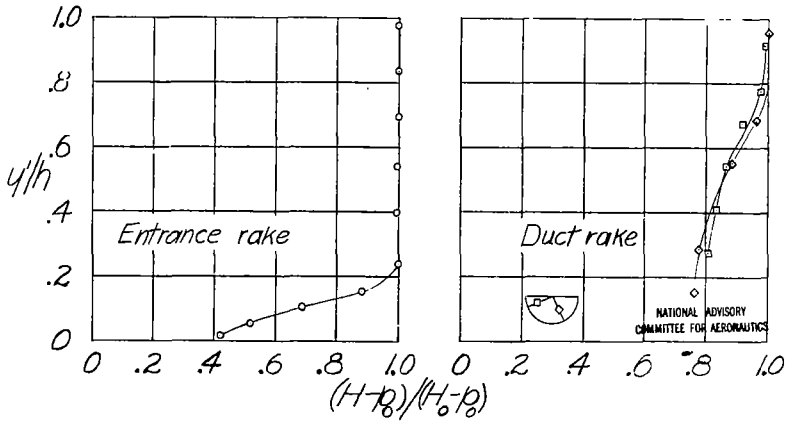

(e) $V_1/V_0 = 0.60$.

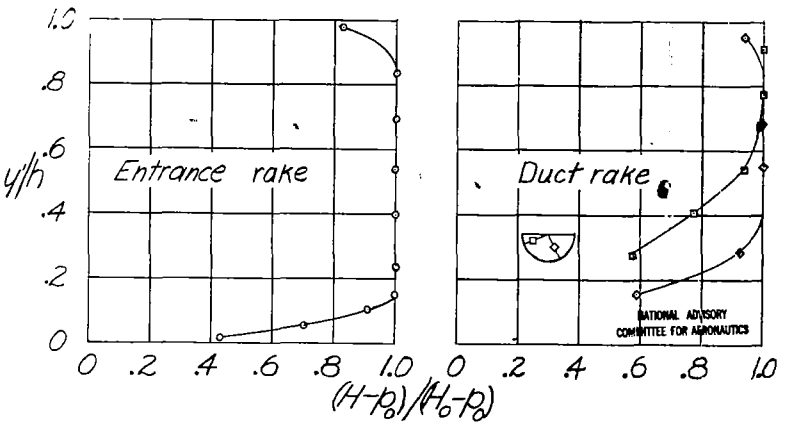

(f) $V_1/V_0 = 0.90$.

Figure 13.- Concluded.

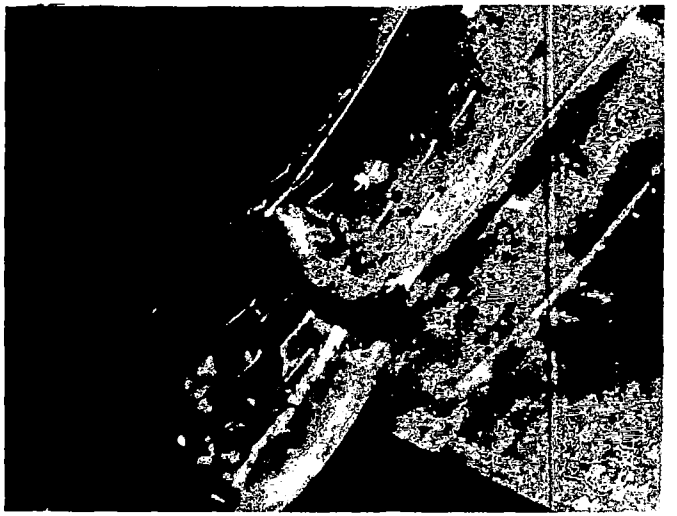

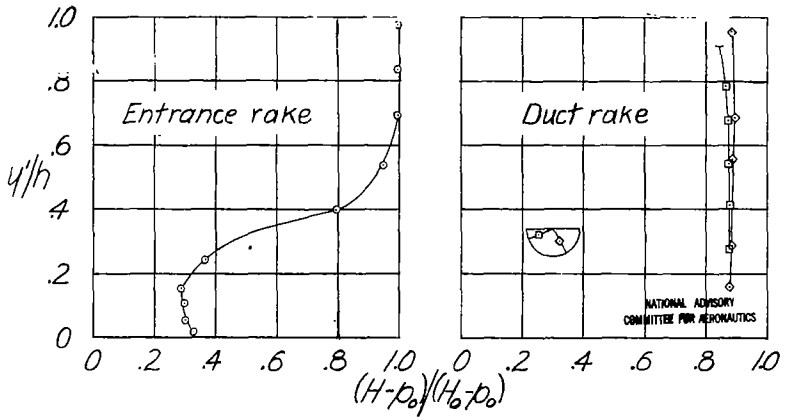

(a) $\alpha = 3°$.

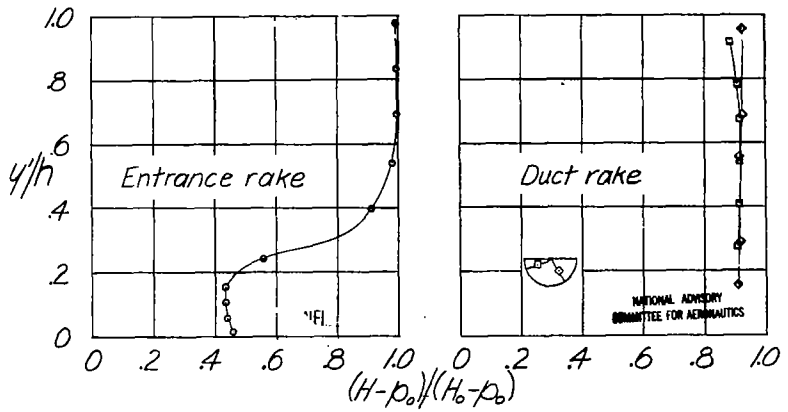

(b) $\alpha = 6°$.

Figure 14.- Tuft photographs and total-pressure recovery profiles for the original scoop for two angles of attack. $\frac{V_1}{V_0} = 0.40$. (Compare with fig. 13(c).)

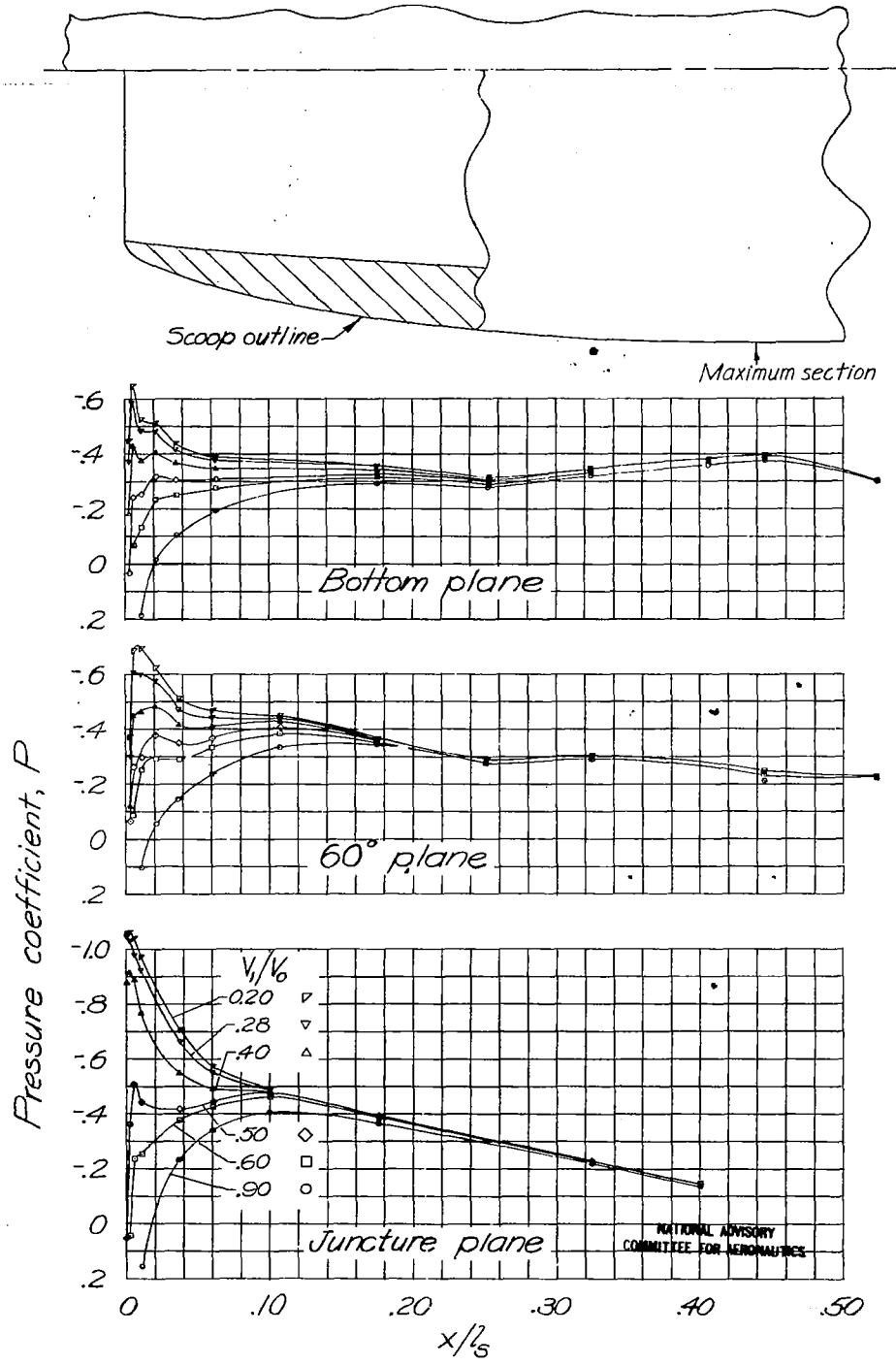

Figure 15.-Pressure distributions over forebody of original scoop. $\alpha = 0°$; $M_0 = 0.40$.

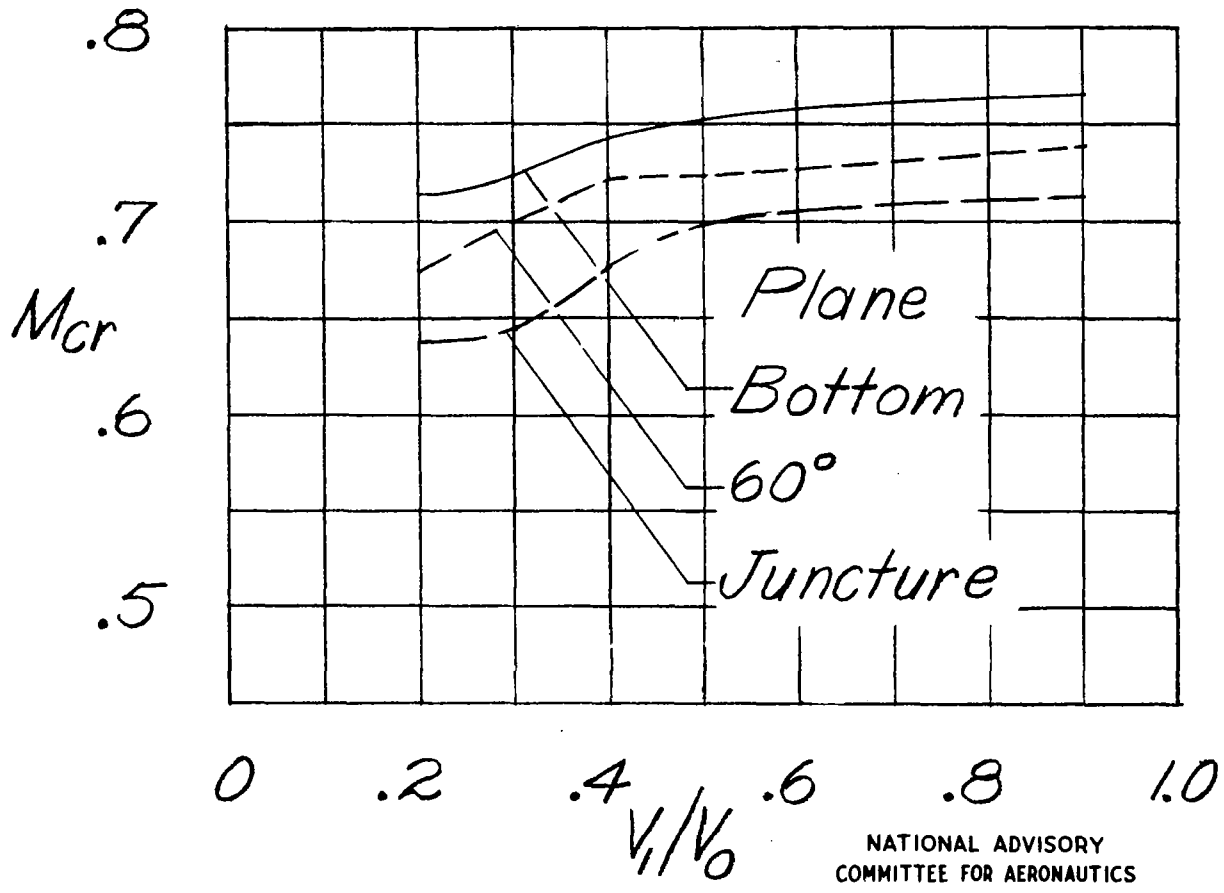

Figure 16.- Critical Mach numbers for original scoop installation. $\alpha = 0°$.

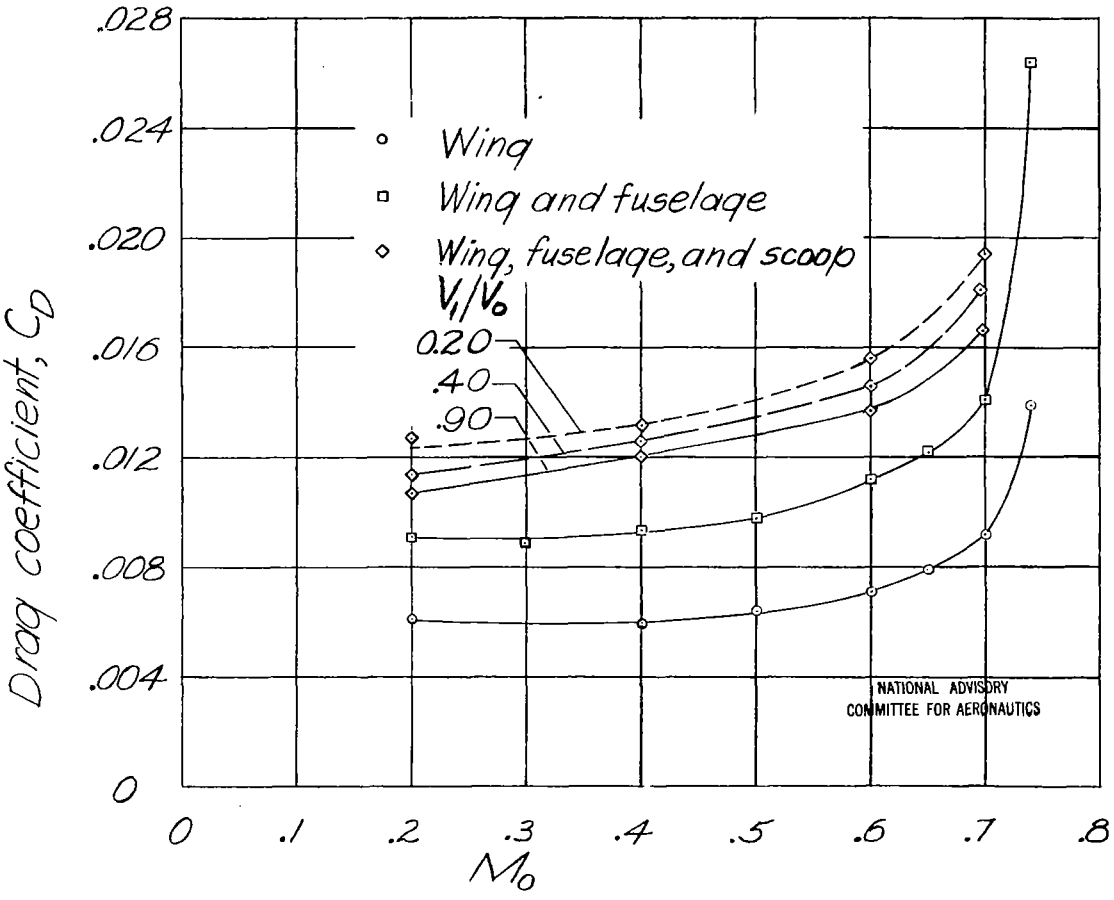

Figure 17.- Drag characteristics of basic model and model with original scoop installation. $\alpha = 0°$.

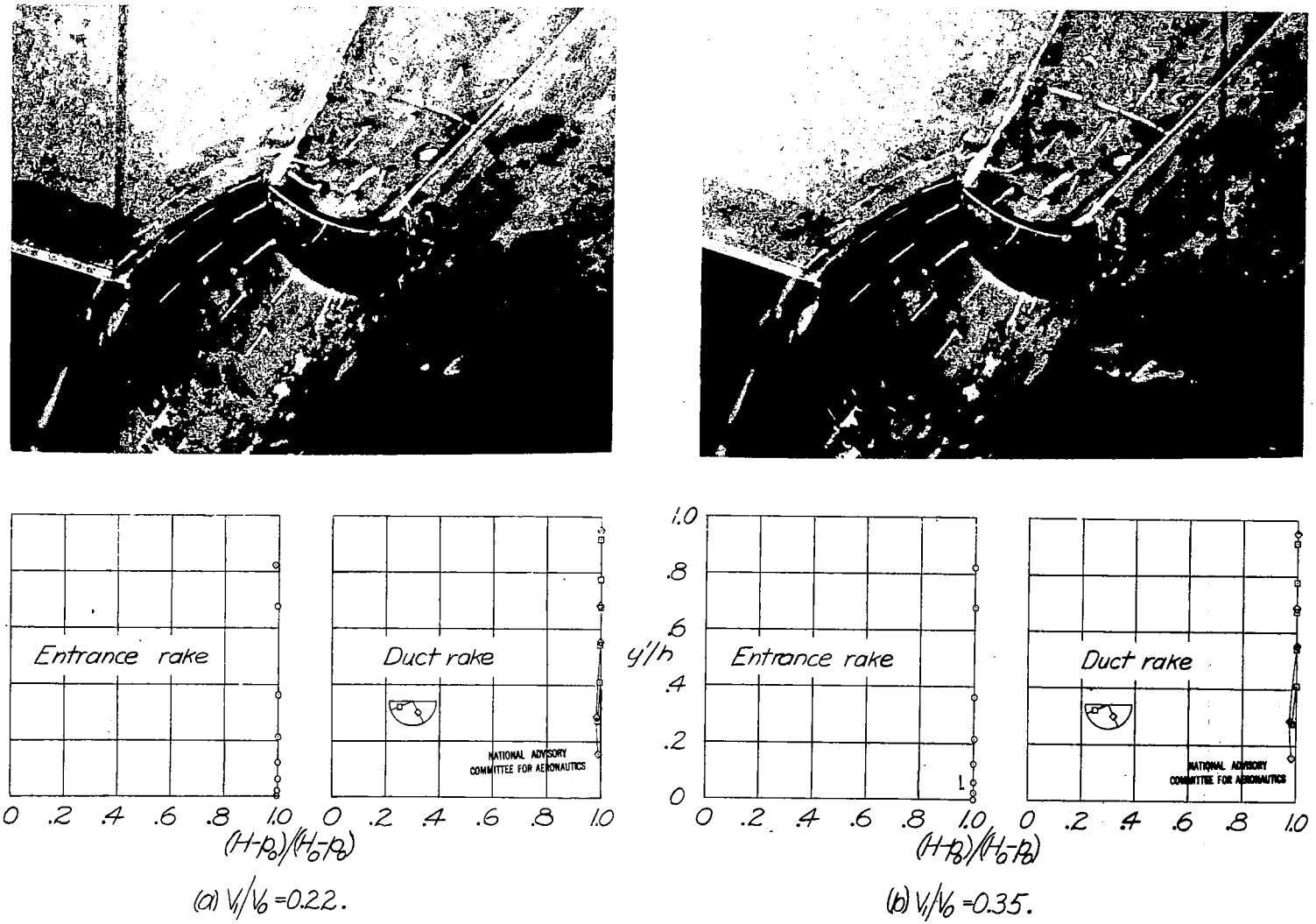

Figure 18.- Tuft photographs and total-pressure-recovery profiles for scoop with boundary-layer passage and partially undercut fuselage. $\alpha = 0^{\circ}$; $M_o = 0.40$; $(V_1/V_o)_{BL} = 0.5$.

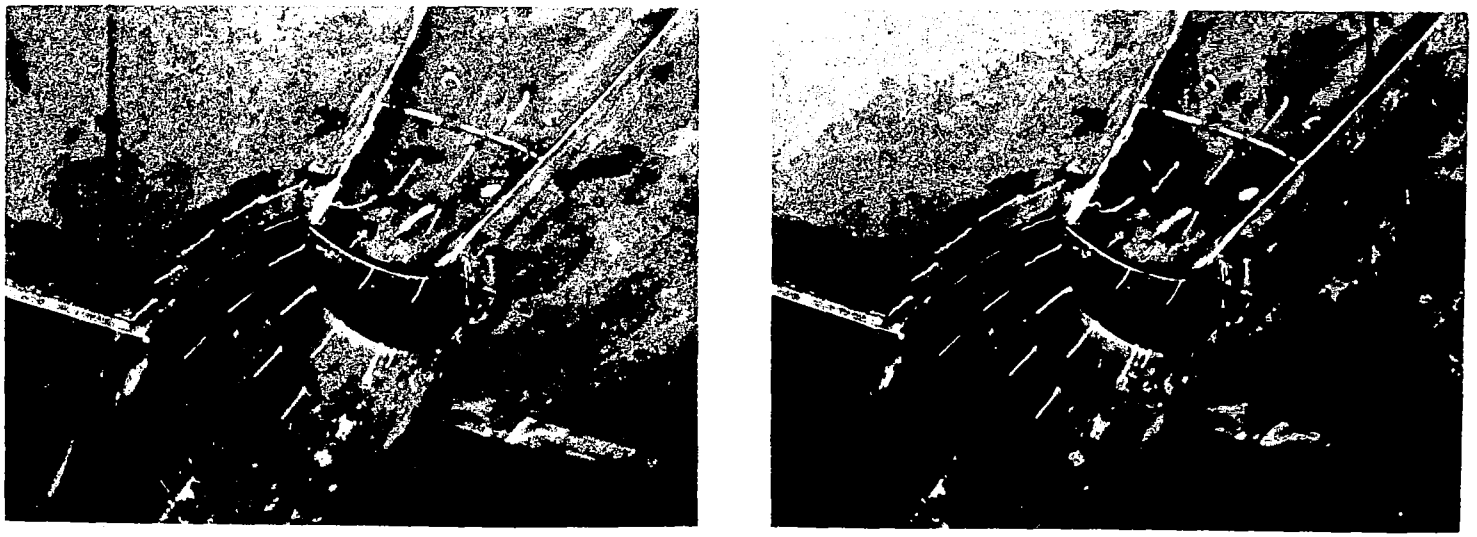

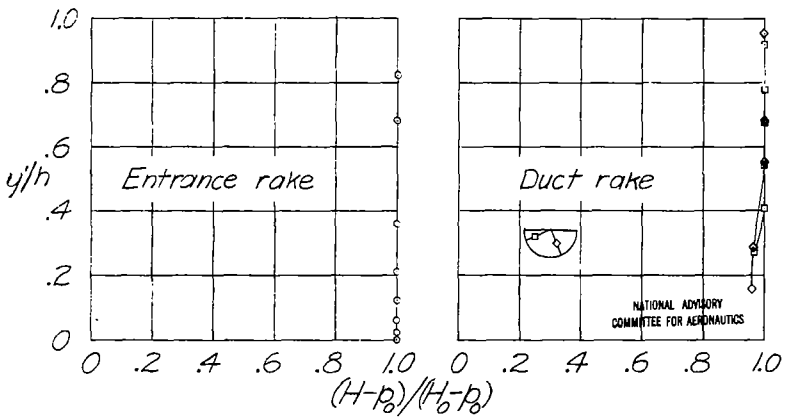

(c) $V_1/V_0 = 0.47$.

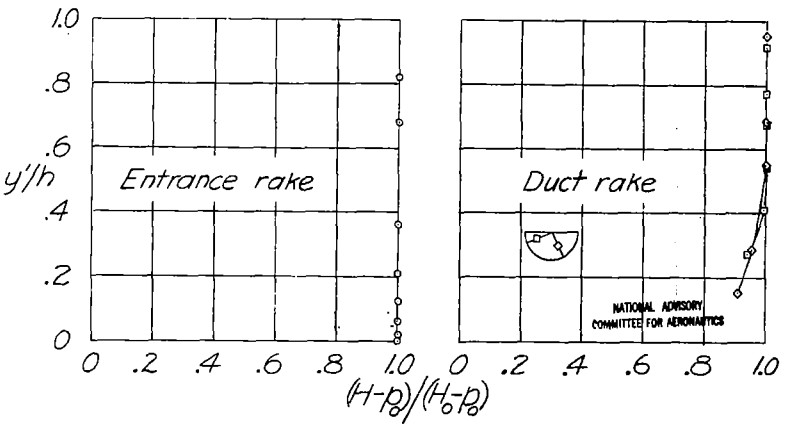

(d) $V_1/V_0 = 0.60$.

Figure 18.- Continued.

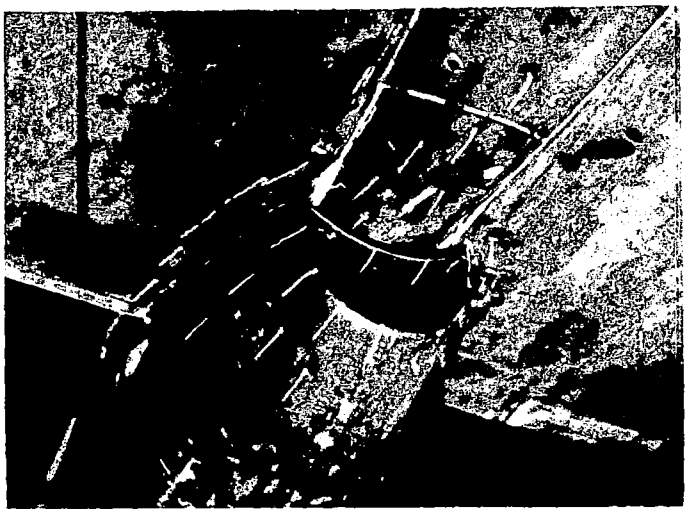

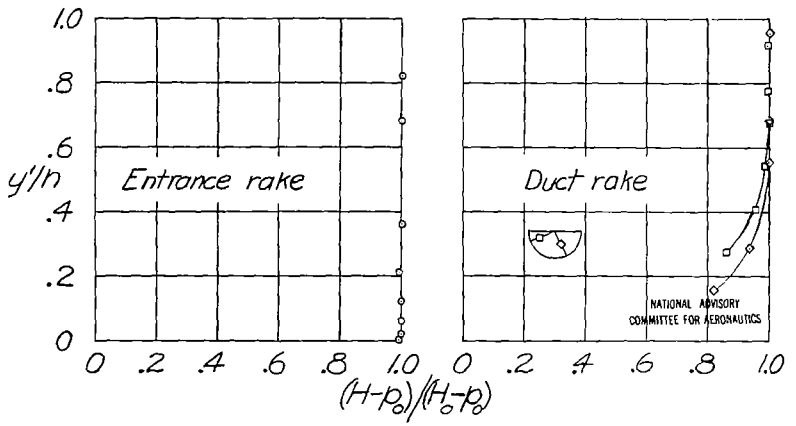

(e) $V_1/V_0 = 0.72$.

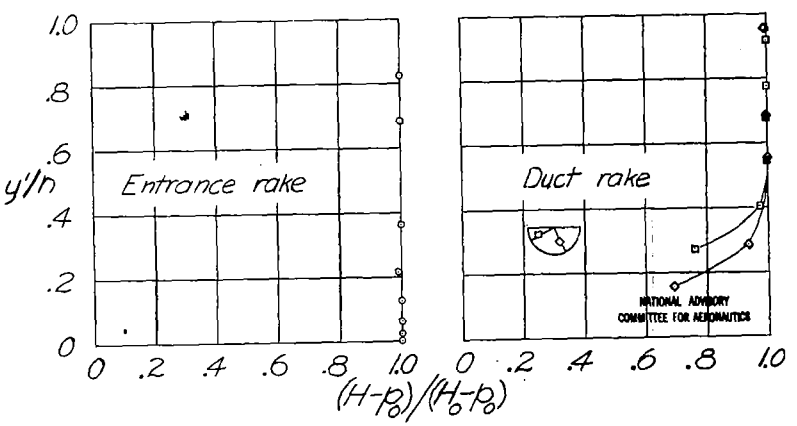

(f) $V_1/V_0 = 1.00$.

Figure 18.- Concluded.

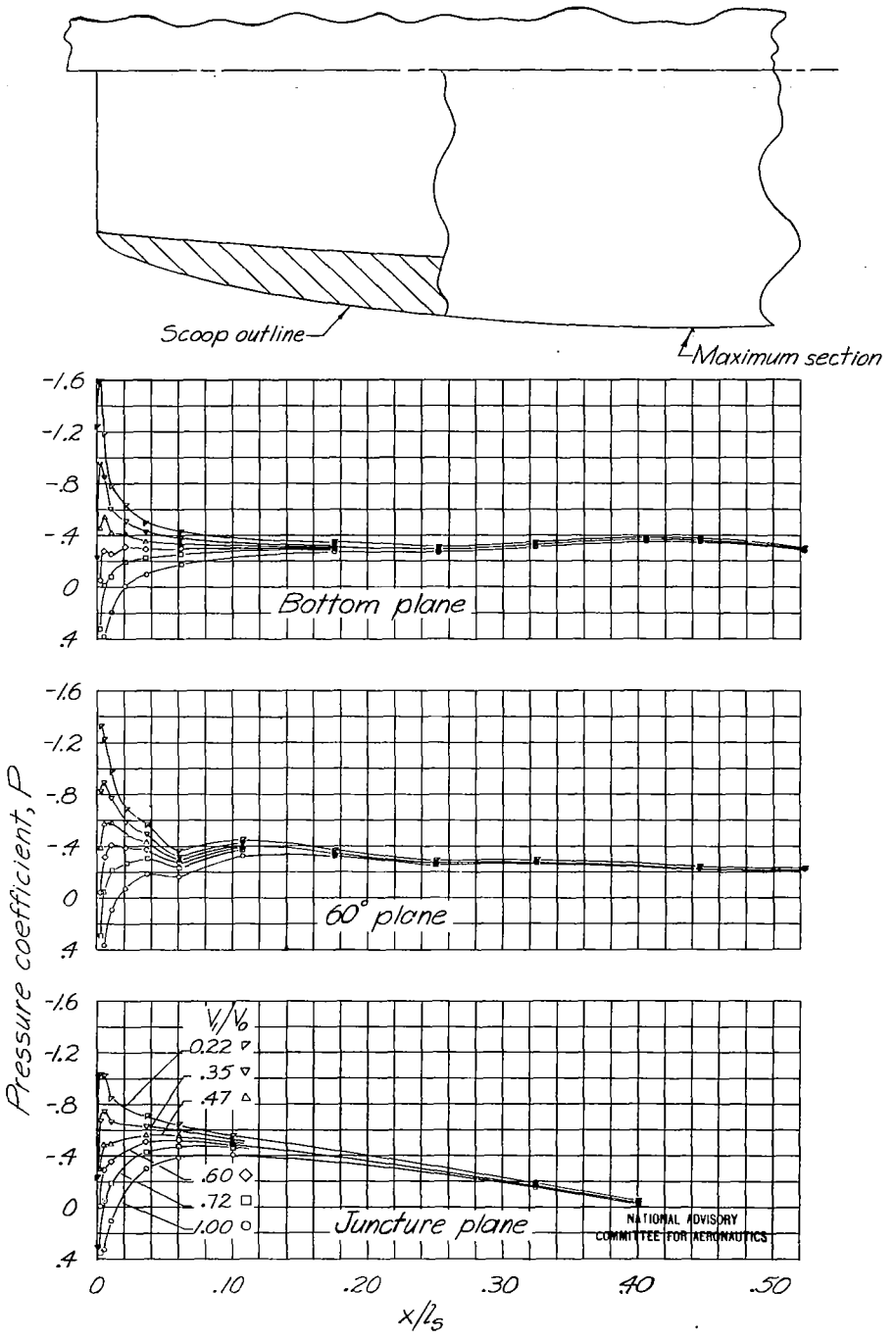

(a) $\alpha = 0°$.

Figure 19.-Pressure distributions over forebody of scoop with boundary-layer passage and partially undercut fuselage. $(V_i/V_0)_{BL}$=0.5; M_0=0.40.

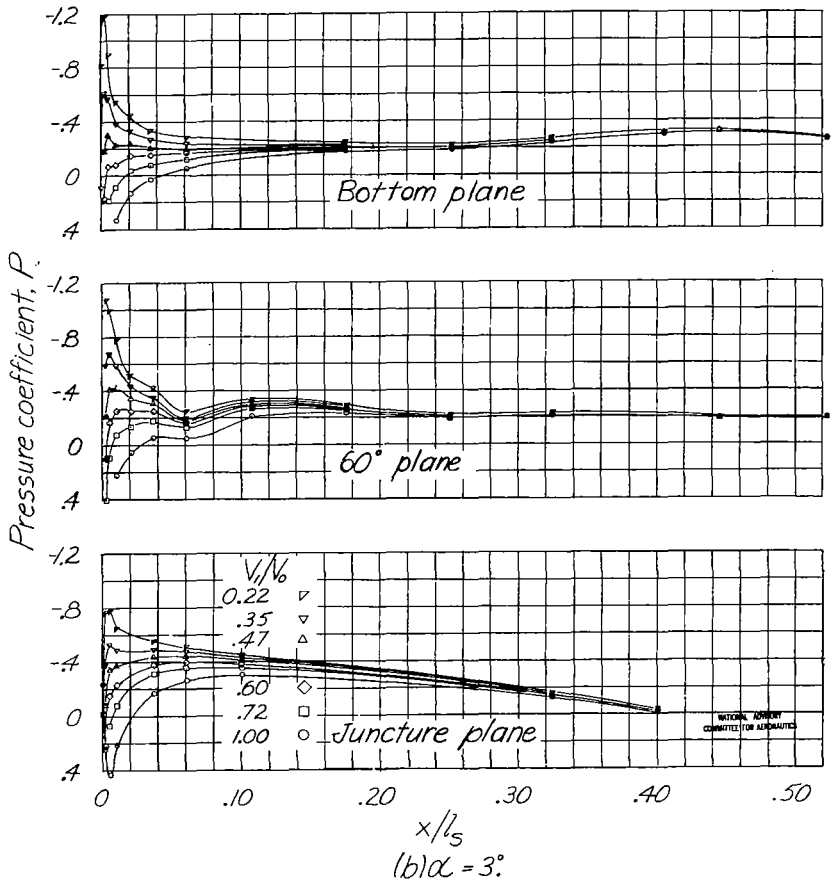

(b) $\alpha = 3°$.

Figure 19.-Concluded.

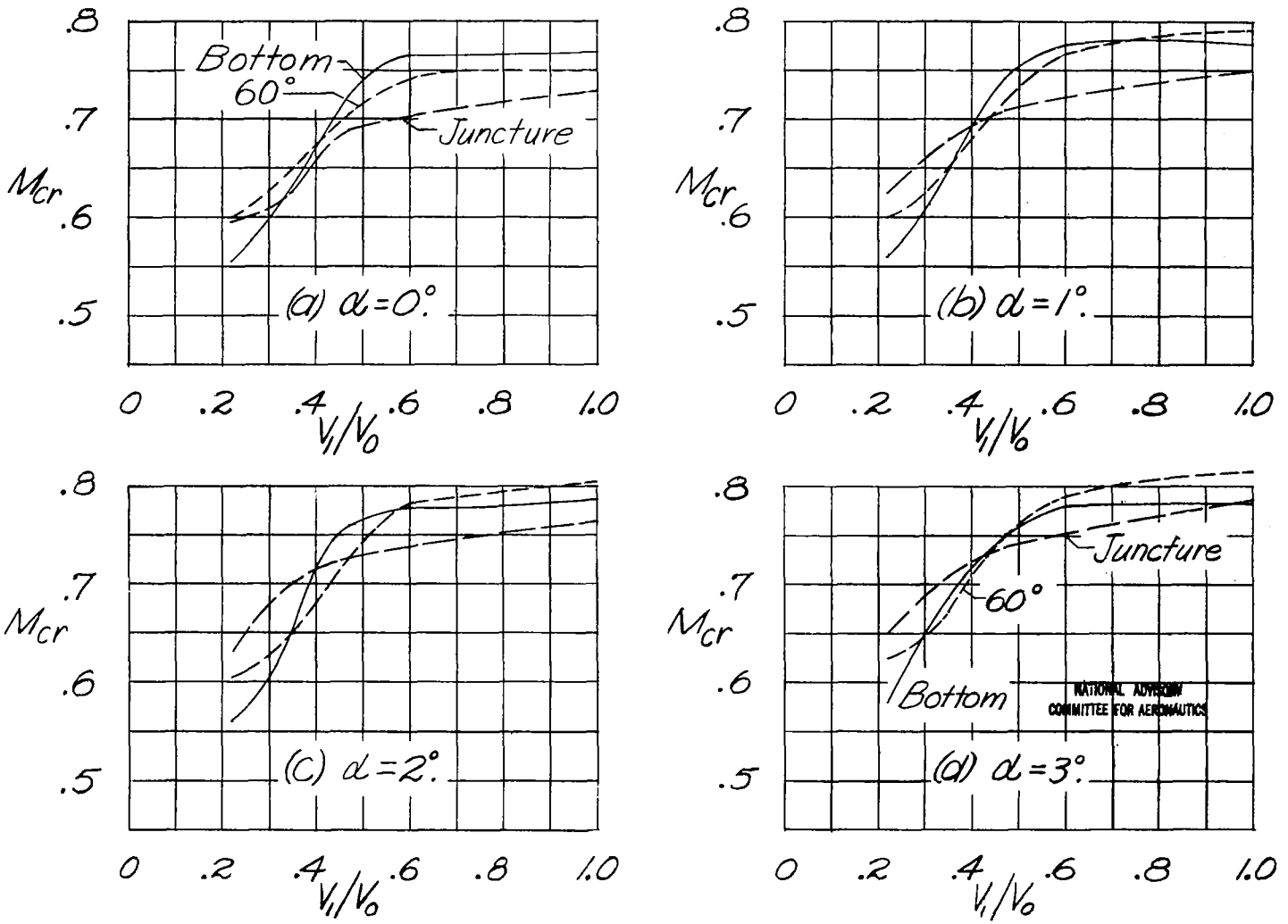

Figure 20.- Critical speeds of scoop with boundary-layer passage and partially undercut fuselage. $(V_1/V_0)_{BL}=0.5$.

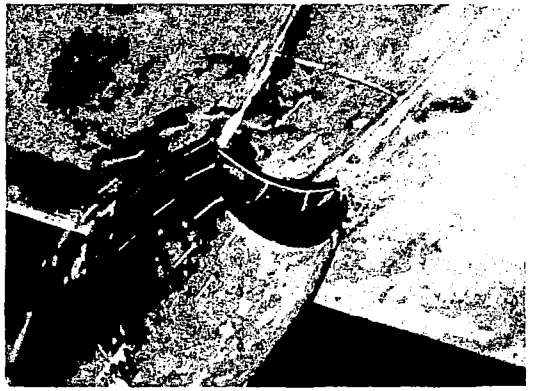

$\frac{V_1}{V_o} = 0.24$

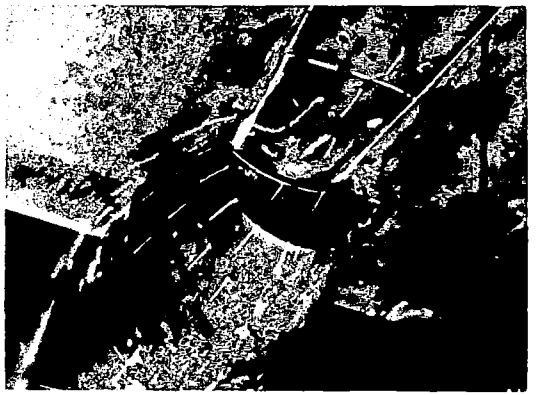

$\frac{V_1}{V_o} = 0.47$

$\frac{V_1}{V_o} = 0.72$

$\frac{V_1}{V_o} = 0.98$

NATIONAL ADVISORY COMMITTEE FOR AERONAUTICS

Figure 21.- Tuft photographs for scoop with boundary-layer passage and partially undercut fuselage. $\alpha = 0^\circ$; $M_o = 0.20$; $(V_1/V_o)_{BL} = 0.2$.

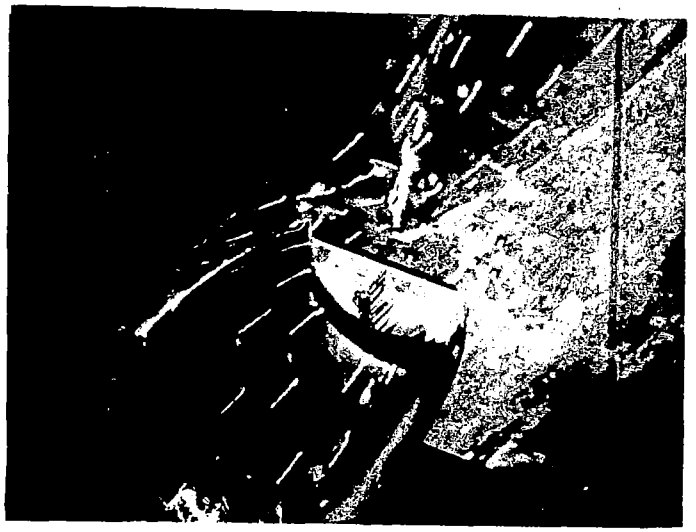

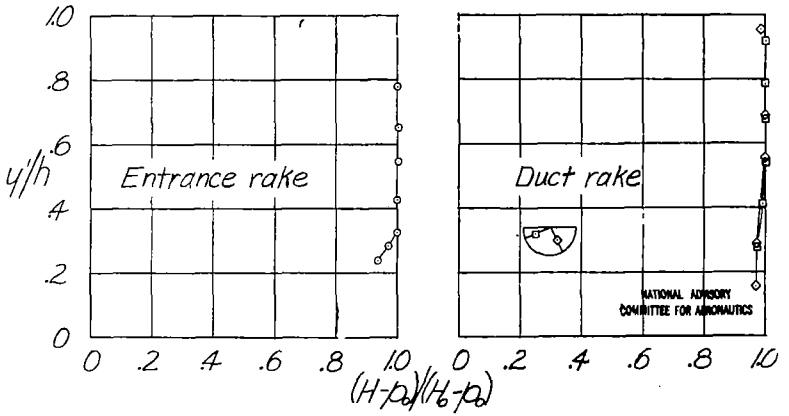

(a) $V_1/V_0 = 0.21$.

(b) $V_1/V_0 = 0.32$.

Figure 22.- Tuft photographs and total-pressure-recovery profiles for scoop with boundary-layer passage and fully undercut fuselage. $\alpha = 0^\circ$; $M_0 = 0.40$; $(V_1/V_0)_{BL} = 0.35$.

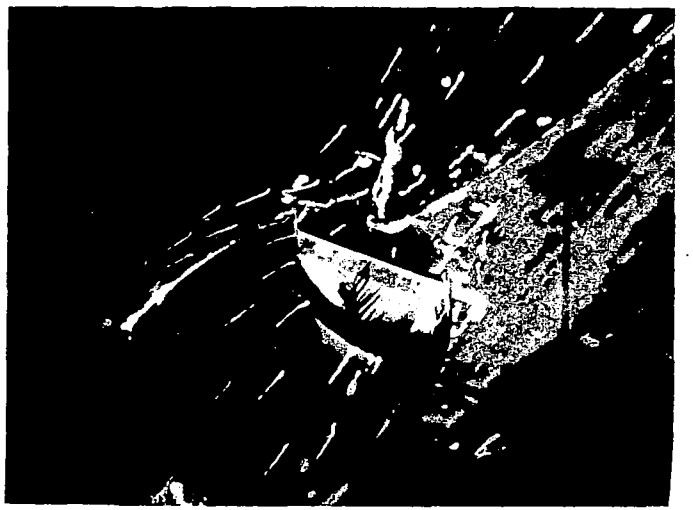

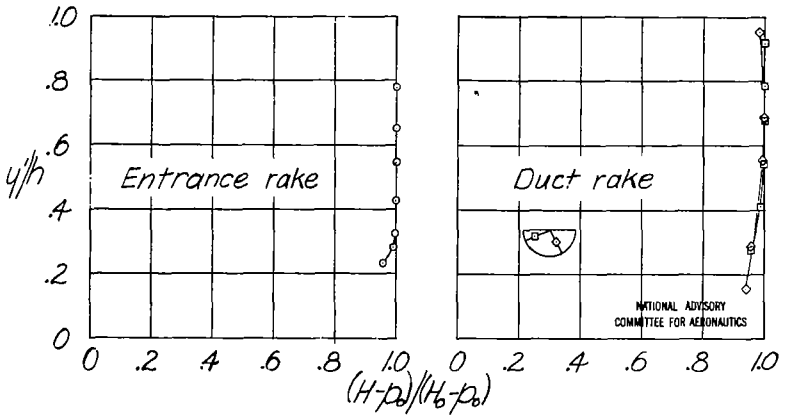

(c) $V_1/V_0 = 0.42$.

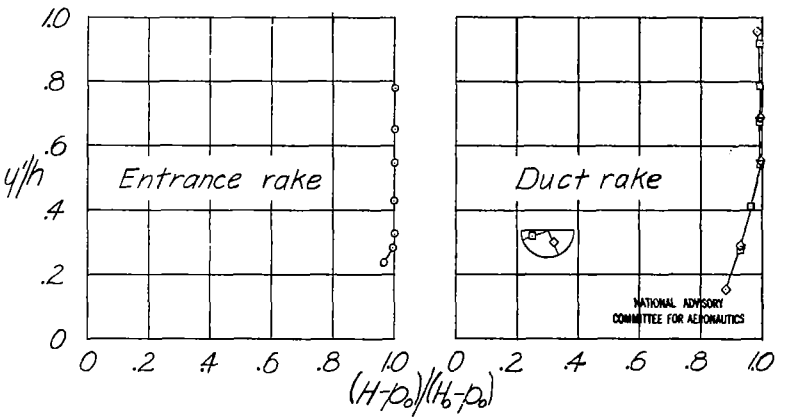

(d) $V_1/V_0 = 0.53$.

Figure 22.- Continued.

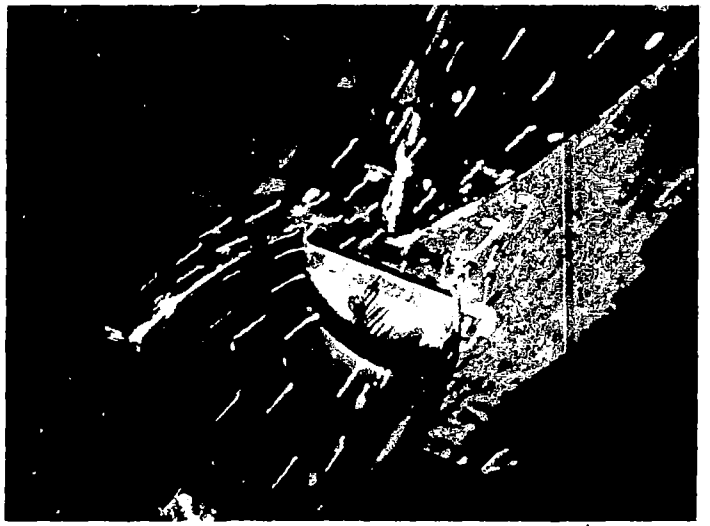

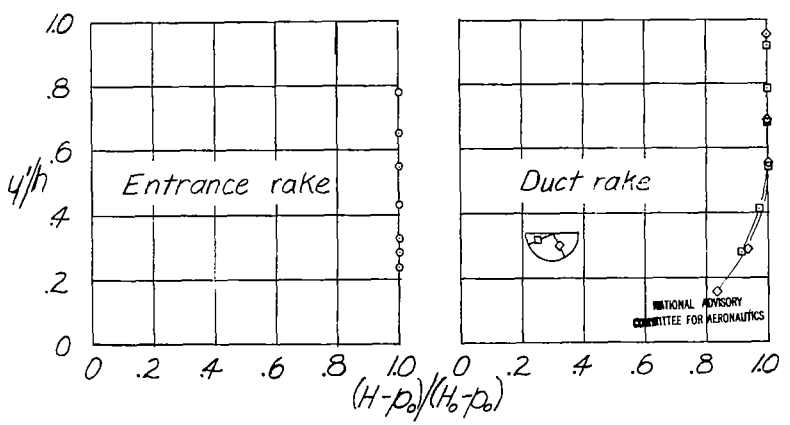

(e) $V_1/V_0 = 0.63$.

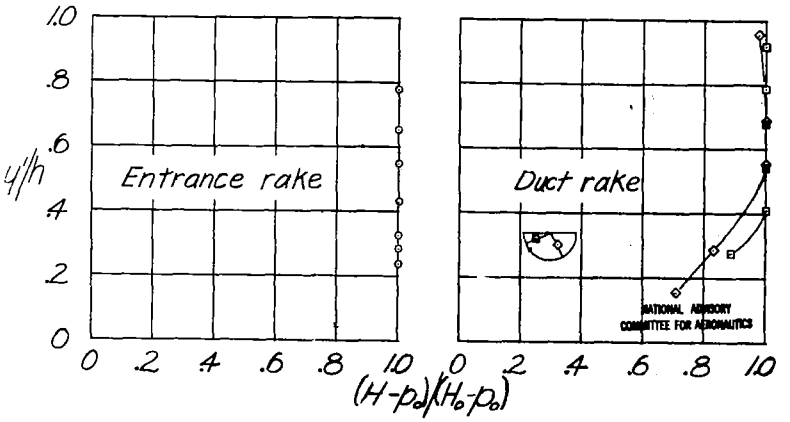

(f) $V_1/V_0 = 0.84$.

Figure 22.- Concluded.

$\frac{V_1}{V_o} = 0.21$

$\frac{V_1}{V_o} = 0.42$

$\frac{V_1}{V_o} = 0.66$

$\frac{V_1}{V_o} = 0.86$

NATIONAL ADVISORY COMMITTEE FOR AERONAUTICS

Figure 23.- Tuft photographs for scoop with boundary-layer passage and fully undercut fuselage. $\alpha = 0^{\circ}$; $M_o = 0.20$; $(V_1/V_o)_{BL} = 0.7$.